

Redox-dependent liver gluconeogenesis impacts different intensity exercise in mice

Received: 14 October 2023

Accepted: 11 August 2025

Published online: 18 September 2025

 Check for updates

Takahiro Horiuchi¹, Keizo Kaneko¹✉, Shinichiro Hosaka¹, Kenji Uno², Seitaro Tomiyama¹, Kei Takahashi¹, Maya Yamato¹, Akira Endo¹, Hiroto Sugawara¹, Yohei Kawana^{1,3}, Yoichiro Asai¹, Shinjiro Kodama¹, Junta Imai¹, Seiya Mizuno⁴, Satoru Takahashi⁴, Atsushi Takasaki⁵, Hiraku Ono^{5,6}, Koutaro Yokote⁷, Rae Maeda⁸, Yuki Sugiura^{8,9} & Hideki Katagiri^{1,3}✉

Hepatic gluconeogenesis produces glucose from various substrates to meet energy demands. However, how these substrates are preferentially used under different conditions remains unclear. Here, we show that preferential supplies of lactate and glycerol modulate hepatic gluconeogenesis, thereby impacting high-intensity and low-intensity exercise capacities, respectively. We find that liver-specific knockout of phosphoenolpyruvate carboxykinase 1 (L-Pck1KO), which blocks gluconeogenesis from lactate, decreases high-intensity exercise capacity but increases low-intensity exercise capacity by enhancing gluconeogenesis from glycerol. Conversely, liver-specific knockout of glycerol kinase (L-GykKO), which inhibits glycerol-derived gluconeogenesis, induces the opposite effects by enhancing gluconeogenesis from lactate. Given that these compensatory steps depend on NAD⁺-mediated oxidation in the cytosol, we hepatically expressed NADH oxidase from *Lactobacillus brevis* (LbNOX) to decrease the cytosolic [NADH]/[NAD⁺] ratio. We find that hepatic LbNOX expression enhances gluconeogenesis from both redox-dependent substrates and increases exercise capacities at both intensities. Importantly, LbNOX-induced enhancement of high-intensity and low-intensity exercise capacities is abolished in L-Pck1KO and L-GykKO mice, respectively. Therefore, supplies of gluconeogenic substrates and cytosolic redox states, rather than altered enzyme expressions, modulate hepatic gluconeogenesis and exercise capacity at different intensities. Globally, this study shows that regulating hepatic gluconeogenesis through cytosolic redox states is a potent strategy for increasing exercise performance.

The liver continuously produces glucose to meet the dramatically changing energy demands of daily activities. Exercise is one of the largest metabolic challenges, wherein muscle adenosine triphosphate (ATP) turnover rates can exceed those at rest by 100-fold¹. During exercise, hepatic gluconeogenesis is highly upregulated, supported by enhanced supplies of gluconeogenic substrates, including lactate and glycerol^{2–4}. Muscle glycolysis, the source of lactate, is highly enhanced in high-intensity exercise where rapid ATP production is

required^{1,5,6}. Meanwhile, adipose lipolysis, the source of glycerol, is more activated in low-intensity than in high-intensity exercise^{7,8}. Although the primary gluconeogenic substrate seems to change depending on exercise intensities, how these gluconeogenic substrates are differentially utilized remains elusive. Here, we aimed to elucidate the physiological importance of hepatic gluconeogenesis utilizing each gluconeogenic substrate during exercise of different intensities.

A full list of affiliations appears at the end of the paper. ✉ e-mail: kayzo@oak.dti.ne.jp; hideki.katagiri.e1@tohoku.ac.jp

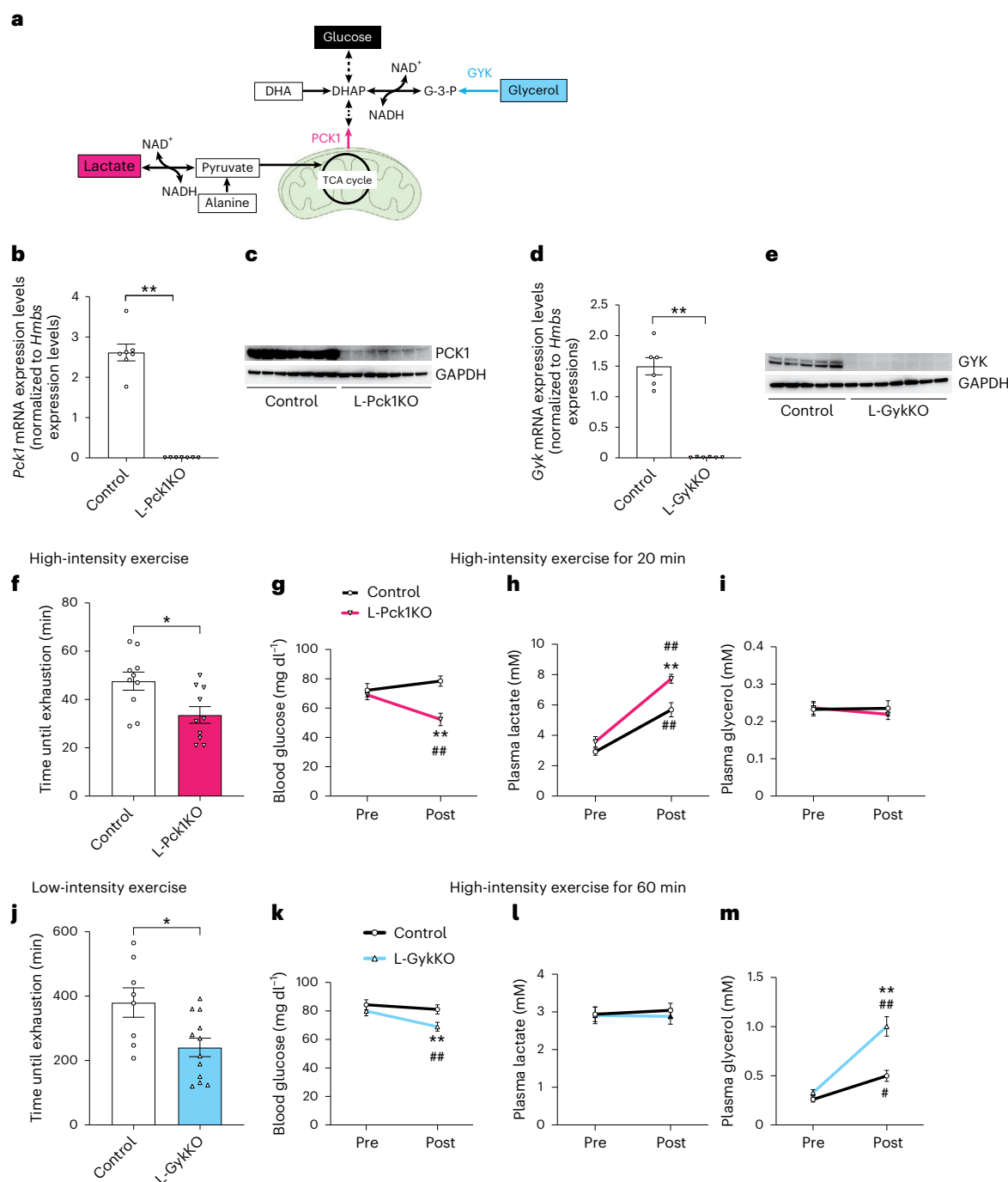


Fig. 1 | L-Pck1KO and L-GykKO decrease high-intensity and low-intensity exercise capacities, respectively. **a**, Schematic diagram of gluconeogenic pathways. Dotted arrows indicate multiple consecutive reactions, while solid arrows indicate a single reaction. The mitochondrion illustration was adapted from BioRender.com. DHAP, dihydroxyacetone phosphate; G-3-P, glycerol-3-phosphate. **b–e**, Expression levels of indicated mRNAs (**b,d**) and western blots for the indicated proteins (**c,e**) in the livers of male L-GykKO or L-Pck1KO mice and the corresponding controls. Signals for each target protein in **c** and **e** were obtained from different membranes that were processed in parallel. $n = 7$ (**b**) and $n = 6$ (**d**) per group; two-tailed unpaired *t*-test; $**P < 0.0001$ (**b**); $**P < 0.0001$ (**d**). **f**, Times until exhaustion in the high-intensity exercise groups of male control and L-Pck1KO mice. $n = 10$ per group; two-tailed unpaired *t*-test; $*P = 0.0134$. **g–i**, Male control and L-Pck1KO mice were subjected to 20 min of high-intensity exercise. Concentrations of blood glucose (**g**), plasma lactate (**h**) and plasma glycerol (**i**) were measured before and after exercise. $n = 9$ for control, $n = 7$

for L-Pck1KO; mixed-effects model followed by Holm–Šidák post hoc analysis (two-sided); $**P = 0.0027$ vs control (post), $^{##}P = 0.0027$ vs pre (within L-Pck1KO) (**in g**); $**P = 0.0035$ vs control (post), $^{##}P < 0.0001$ vs pre (within L-Pck1KO), $^{##}P = 0.0001$ vs pre (within control) (**in h**). **j**, Times until exhaustion in the low-intensity exercise groups of male control and L-GykKO mice. $n = 8$ for control, $n = 12$ for L-GykKO; two-tailed unpaired *t*-test; $*P = 0.0138$. **k–m**, Male control and L-GykKO mice were subjected to 60 min of low-intensity exercise. Concentrations of blood glucose (**k**), plasma lactate (**l**) and plasma glycerol (**m**) were measured before and after exercise. $n = 12$ per group; repeated measures two-way ANOVA followed by Holm–Šidák post hoc analysis (two-sided); $**P = 0.0022$ vs control (post), $^{##}P = 0.0035$ vs pre (within L-GykKO) (**in k**); $**P = 0.0001$ vs control (post), $^{##}P < 0.0001$ vs pre (within L-GykKO), $^{#}P = 0.0204$ vs pre (within control) (**in m**). Experiments shown in **b,c,d,e,f,g–i,j** and **k–m** were conducted using distinct cohorts of biologically independent mice. All data are presented as means; error bars, s.e.m. Each plot on the bar graph shows raw data.

Given that blood lactate levels of wild-type mice reportedly rise at running speeds higher than 20 m min⁻¹ (ref. 9), we conducted treadmill exercise experiments at up to 25 m min⁻¹ as high-intensity and at 13 m min⁻¹ as low-intensity exercise. As expected, in wild-type mice, 20 min of high-intensity exercise raised concentrations of plasma lactate but not plasma glycerol or blood glucose (Extended Data Fig. 1a–c). By contrast, 60 min of low-intensity exercise significantly increased plasma glycerol without changing plasma lactate and blood glucose levels (Extended Data Fig. 1d–f). Thus, lactate and glycerol supplies exceed their utilization in high-intensity and low-intensity exercise, respectively.

Phosphoenolpyruvate carboxykinase 1 (PCK1) and glycerol kinase (GK) are the key enzymes for gluconeogenic pathways utilizing lactate and glycerol, respectively (Fig. 1a). To separately block hepatic gluconeogenesis from each substrate, we generated mice with tamoxifen-inducible liver-specific PCK1 knockout (L-Pck1KO) and GK knockout (L-GykKO). After tamoxifen treatment, the respective target genes and proteins were barely detectable in each of the knockout mouse livers (Fig. 1b–e), with minimally altered expressions in other organs and tissues (Extended Data Fig. 2a–d). Except for the greater liver weights in L-Pck1KO mice, as previously reported¹⁰, body compositions, blood glucose and liver glycogen contents in both knockout mice were similar to those of the corresponding controls (Extended Data Fig. 2e–p). Therefore, the effects of L-Pck1KO and L-GykKO were not enough to change blood glucose levels under sedentary conditions.

By contrast, L-Pck1KO and L-GykKO mice showed decreased exercise capacities for high-intensity and low-intensity exercise, respectively (Fig. 1f, j). To ensure comparability, we fixed the exercise durations to 20 min and 60 min for high-intensity and low-intensity exercise, respectively, when none of the mice stopped exercising. L-Pck1KO and L-GykKO mice after high-intensity and low-intensity exercise showed decreased blood glucose with increased plasma lactate and glycerol levels, respectively, whereas other energy sources (alanine, fatty acids and ketone bodies) were unchanged compared to those of control mice (Fig. 1g–i, k–m and Extended Data Fig. 3a–f). These observations probably reflect the inability of PCK1-deficient and GK-deficient hepatocytes to use lactate and glycerol, respectively, for gluconeogenesis. Therefore, hepatic gluconeogenesis from lactate via PCK1 and glycerol via GK serves as a major energy source during high-intensity and low-intensity exercise, respectively.

Surprisingly, L-Pck1KO significantly increased low-intensity exercise capacities by approximately 100 min on average (Fig. 2a). After 60 min of low-intensity exercise, L-Pck1KO mice exhibited increased blood glucose levels with less of a rise in plasma glycerol and no changes in other energy sources compared to control mice (Fig. 2b, d and Extended Data Fig. 3g–i). These results indicate that L-Pck1KO reciprocally enhanced gluconeogenesis from glycerol during low-intensity exercise. Again, intriguingly, L-GykKO increased high-intensity exercise capacities (Fig. 2e). In L-GykKO mice, 20 min of high-intensity exercise increased blood glucose levels with more modest elevations in plasma lactate and no changes in other energy sources compared to control mice (Fig. 2f, g and Extended Data Fig. 3j–l), indicating reciprocally enhanced gluconeogenesis from lactate in L-GykKO mice. Plasma lactate and glycerol in L-Pck1KO and L-GykKO mice were slightly increased after low-intensity and high-intensity exercise, respectively (Fig. 2c, h), suggesting an inability to use slightly increased supplies of these substrates. Collectively, PCK1 and GK deletion may enhance gluconeogenesis from the unblocked alternative pathway during low-intensity and high-intensity exercise, respectively.

We further evaluated the metabolic flux, under sedentary and exercised conditions, of the models with enhanced exercise capacities (that is, L-Pck1KO and L-GykKO mice during low-intensity and high-intensity exercise, respectively) (Fig. 2i). Glucose rates of appearance showed no significant difference in L-Pck1KO or L-GykKO mice compared to the corresponding controls under sedentary conditions (Fig. 2j, l). Notably, although exercise of both intensities increased glucose rates of appearance in control mice, those of knockout mice rose further (Fig. 2j, l). These results strongly corroborate our hypothesis that gluconeogenesis is upregulated in L-Pck1KO mice during low-intensity exercise and in L-GykKO mice during high-intensity exercise. Furthermore, plasma ¹³C-labelled glucose, which is derived from [¹³C₃]glycerol and [¹³C₃]lactate, was higher in L-Pck1KO and L-GykKO mice during low-intensity and high-intensity exercise, respectively, than in the corresponding controls (Fig. 2k, m). Therefore, L-Pck1KO and L-GykKO enhanced gluconeogenesis from glycerol during low-intensity exercise and from lactate during high-intensity exercise, respectively, leading to reciprocally increased exercise capacities.

Next, we endeavoured to elucidate the mechanism(s) underlying the reciprocal enhancements of gluconeogenesis in each type of knockout mouse. mRNA and protein expression levels of hepatic gluconeogenic enzymes were similar in each type of knockout mouse and

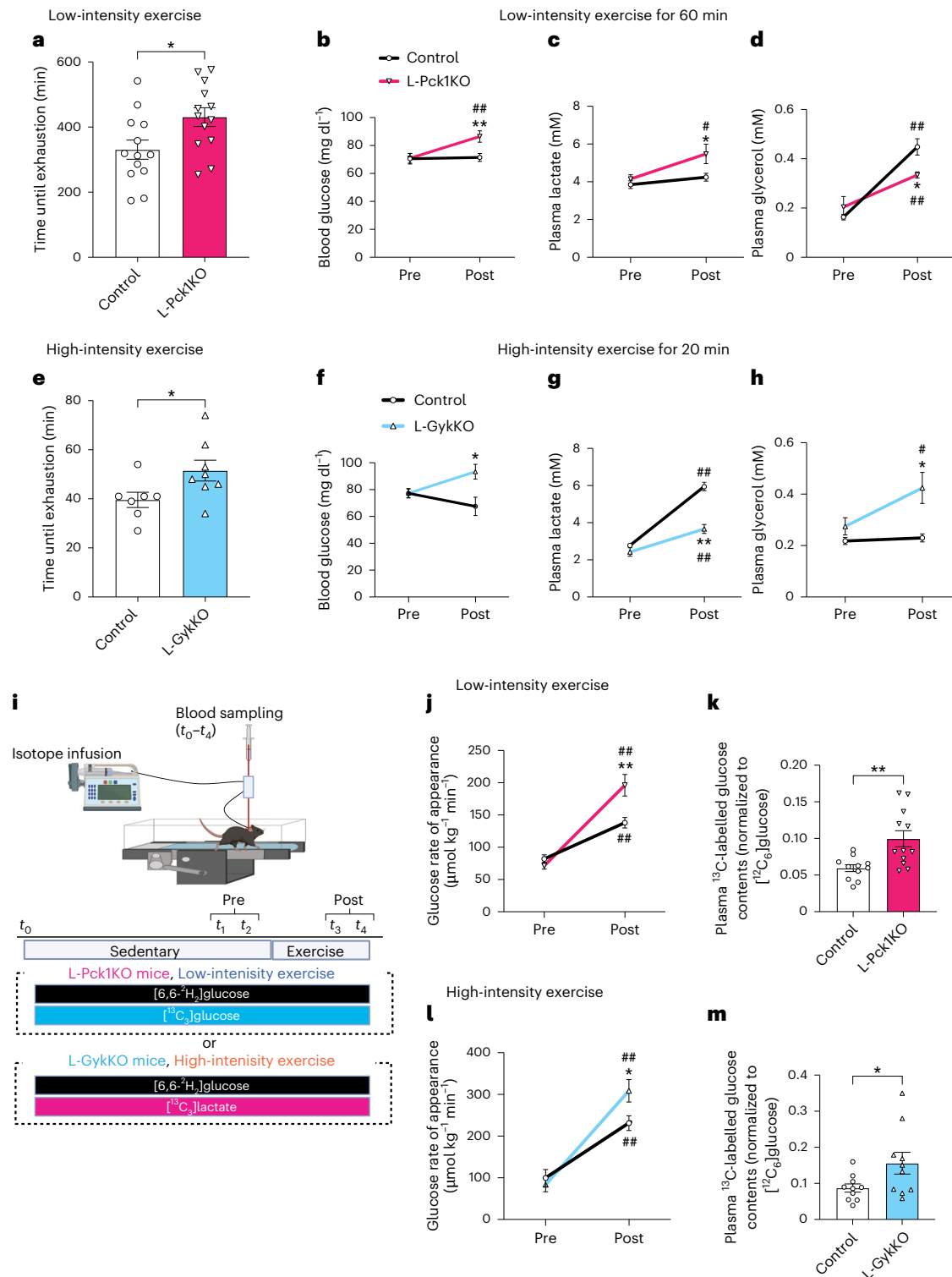
Fig. 2 | L-Pck1KO and L-GykKO increase low-intensity and high-intensity exercise capacities with enhanced gluconeogenesis from glycerol and lactate, respectively.

a, Times until exhaustion in the low-intensity exercise groups of male control and L-Pck1KO mice. $n = 13$ per group; two-tailed unpaired t -test; $*P = 0.0232$. **b–d**, Male control and L-Pck1KO mice were subjected to 60 min of low-intensity exercise. Concentrations of blood glucose (**b**), plasma lactate (**c**) and plasma glycerol (**d**) were measured before and after exercise. $n = 9$ (in **b**) and 12 (in **c** and **d**) per group; repeated measures two-way ANOVA followed by Holm–Šidák post hoc analysis (two-sided); $**P = 0.0089$ vs control (post), $^{##}P = 0.0089$ vs pre (within L-Pck1KO) (in **b**); $*P = 0.0364$ vs control (post), $^{##}P = 0.0328$ vs pre (within L-Pck1KO) (in **c**); $*P = 0.0145$ vs control (post), $^{##}P = 0.0097$ vs pre (within L-Pck1KO) (in **d**); $^{##}P < 0.0001$ vs pre (within control) (in **d**). **e**, Times until exhaustion in the high-intensity exercise groups of male control and L-GykKO mice. $n = 7$ for control, $n = 8$ for L-GykKO; two-tailed unpaired t -test; $*P = 0.0458$. **f–h**, Male control and L-GykKO mice were subjected to 20 min of high-intensity exercise. Concentrations of blood glucose (**f**), plasma lactate (**g**) and plasma glycerol (**h**) were measured before and after exercise. $n = 8$ per group (in **f**); $n = 6$ for control, $n = 9$ for L-GykKO (in **g** and **h**); repeated measures two-way ANOVA (in **f**) or mixed-effects model (in **g** and **h**) followed by Holm–Šidák post hoc analysis (two-sided); $*P = 0.0357$ vs control (post) (in **f**); $**P < 0.0001$ vs control (post), $^{##}P = 0.0011$ vs pre (within L-GykKO), $^{##}P < 0.0001$ vs pre (within control) (in **g**); $*P = 0.0307$ vs control (post), $^{##}P = 0.0159$ vs pre (within L-GykKO) (in **h**). **i**, Schematic representation of isotopic metabolic flux analysis during exercise. The detailed protocols are described in the Methods. Male control and L-Pck1KO

mice received prime and continuous infusions of [6,6-²H₂]glucose and [¹³C₃]glycerol starting 210 min before low-intensity exercise. Male control and L-GykKO mice received prime and continuous infusions of [6,6-²H₂]glucose and [¹³C₃]lactate starting 210 min before high-intensity exercise. Blood was collected at times t_0 – t_5 . After correcting isotopic enrichment with naturally occurring isotopes from t_0 , metabolic flux under sedentary conditions was calculated using data from t_1 and t_2 , while metabolic flux during exercise was determined by t_3 and t_4 . The schematic diagram was created in BioRender.com. **j, l**, The glucose rate of appearance (Ra) was estimated before and during low-intensity exercise in control and L-Pck1KO mice (**j**) or high-intensity exercise in control and L-GykKO mice (**l**). $n = 11$ for control, $n = 12$ for L-Pck1KO (in **j**); $n = 10$ per group (in **l**); mixed-effects model (in **j**) or repeated measures two-way ANOVA (in **l**) followed by Holm–Šidák post hoc analysis (two-sided); $**P = 0.0060$ vs control (post), $^{##}P < 0.0001$ vs pre (within L-Pck1KO), $^{##}P = 0.0060$ vs pre (within control) (in **j**); $*P = 0.0407$ vs control (post), $^{##}P < 0.0001$ vs pre (within L-GykKO), $^{##}P = 0.0031$ vs pre (within control) (in **l**). **k, m**, Plasma contents of ¹³C-labelled glucose with normalization to [¹²C₆]glucose were calculated during low-intensity exercise in control and L-Pck1KO mice (**k**) or high-intensity exercise in control and L-GykKO mice (**m**). $n = 11$ for control, $n = 12$ for L-Pck1KO (in **k**); $n = 10$ per group (in **m**); two-tailed unpaired t -test; $*P = 0.0040$ (in **k**); $*P = 0.0074$ (in **m**). Experiments shown in **a, b, c, d, e, f, g, h, j, k** and **l, m** were conducted using distinct cohorts of biologically independent mice. All data are presented as means; error bars, s.e.m. Each plot on the bar graph shows raw data.

the corresponding controls, except for increased GYK in L-Pck1KO mice (Extended Data Fig. 4a–d). We then performed a series of tolerance tests specific to various gluconeogenic substrates. As expected, compared to control mice, blood glucose levels were decreased after administering substrates requiring one of the knocked-out enzymes in their gluconeogenic pathways (lactate, pyruvate and alanine in L-Pck1KO mice, and glycerol in L-GykKO mice) (Extended Data Fig. 4e–h). L-GykKO and control mice showed similar glycaemia after administering dihydroxyacetone (DHA) (Extended Data Fig. 4i). Notably, blood glucose levels of L-Pck1KO mice were more elevated than those of control mice

after administration of glycerol, but not DHA, suggesting that the step from glycerol to dihydroxyacetone phosphate was enhanced in L-Pck1KO mice (Fig. 3a–c). By contrast, L-GykKO mice showed a greater increase in glycaemia than control mice after administration of lactate, but not pyruvate or alanine, suggesting enhancement of the converting step from lactate to pyruvate in L-GykKO mice (Fig. 3c–f). Interestingly, both of the enhanced steps are redox-dependent; namely, dependent on the conversion of the oxidized form of cytosolic nicotinamide dinucleotide (NAD⁺) into its reduced form (NADH). Therefore, we reasoned that L-Pck1KO and L-GykKO had altered hepatic cytosolic



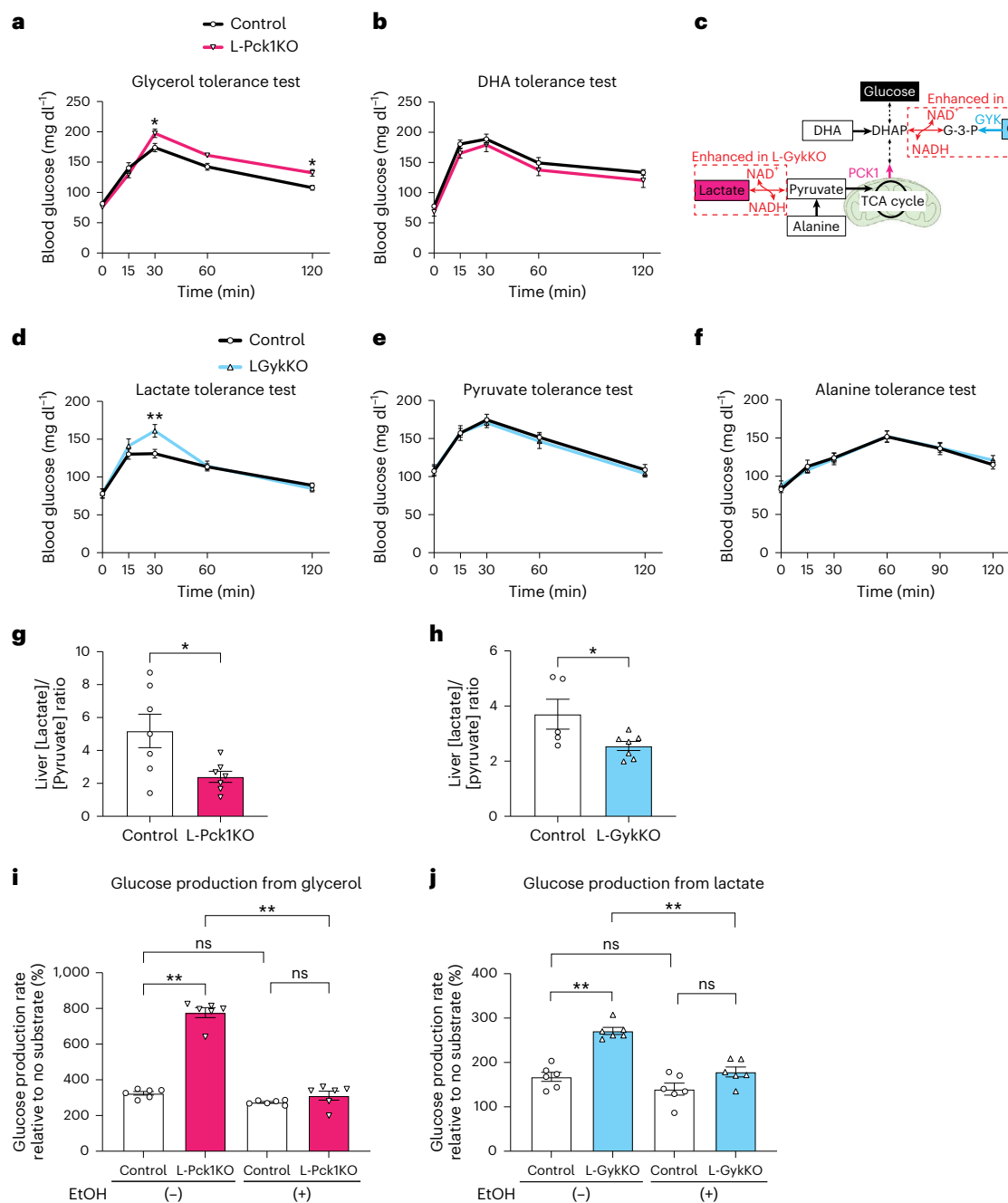


Fig. 3 | Hepatic cytosolic redox states mediate the enhanced gluconeogenesis from glycerol in L-Pck1KO mice and lactate in L-GykKO mice. a, b, d–f, Blood glucose levels of male L-Pck1KO (a, b) or L-GykKO (d–f) mice in comparison with the corresponding controls after intraperitoneal administrations of the indicated gluconeogenic substrates. $n = 7$ for control, $n = 6$ for L-Pck1KO (in a); $n = 8$ per group (in b and d–f); mixed-effects model (in a) or repeated measures two-way ANOVA (in b and d–f) followed by Holm–Šidák post hoc analysis (two-sided); * $P = 0.0311$ and 0.0292 vs control (at 30 and 120 min, respectively) (in a); ** $P = 0.0020$ vs control (at 30 min) (in d). c, Schematic image of gluconeogenic pathways. The enhanced steps in each type of knockout mouse, suggested by the series of substrate tolerance tests, are indicated by red dotted lines. The mitochondrion illustration was adapted from [BioRender.com](https://www.biorender.com). g, h, The liver

[lactate]/[pyruvate] ratios of male L-Pck1KO mice (g) and L-GykKO mice (h) are shown in comparison to those of the corresponding controls. $n = 7$ per group (in g); $n = 5$ for control, $n = 7$ for L-GykKO (in h); two-tailed unpaired t -test; * $P = 0.0168$ (in g); * $P = 0.0404$ (in h). i, j, Glucose production in response to glycerol in primary hepatocytes isolated from male L-Pck1KO mice (i) and to lactate in primary hepatocytes isolated from male L-GykKO mice (j) were compared to those of the corresponding controls under the conditions with or without ethanol (EtOH) treatment. $n = 6$ per group; one-way ANOVA followed by Tukey's post hoc analysis (two-sided); ** $P < 0.0001$. All experiments shown in a–j were conducted using distinct cohorts of biologically independent mice. All data are presented as means; error bars, s.e.m. Each plot on the bar graph shows raw data.

redox states, which in turn enhanced gluconeogenesis from glycerol and lactate, respectively. Cytosol-specific NAD(H) concentrations were unmeasurable because of the difficulty involved with removing the major NAD(H) pool in the mitochondria and distinguishing free NAD(H) from protein-binding forms¹¹. Indeed, L-Pck1KO and L-GykKO did not

alter the whole-liver [NADH]/[NAD⁺] ratios (Extended Data Fig. 4j, m). We therefore measured the hepatic [lactate]/[pyruvate] ratio, a reliable and functional indicator of the cytosolic [NADH]/[NAD⁺] ratio^{11–14}. In agreement with our hypothesis, hepatic [lactate]/[pyruvate] ratios in both L-Pck1KO and L-GykKO mice were significantly decreased

compared to those of the corresponding controls (Fig. 3g,h and Extended Data Fig. 4j–m). Furthermore, in ex vivo experiments using isolated primary hepatocytes, the increased glucose production from glycerol in PCK1-deleted hepatocytes and from lactate in GYK-deleted hepatocytes was abrogated by ethanol treatment, which reportedly converts NAD⁺ into NADH^{15,16} (Fig. 3i,j). These findings clearly indicate that increased gluconeogenesis from redox-dependent substrates through the alternative unblocked gluconeogenic pathway is mainly caused by the decreased hepatic cytosolic [NADH]/[NAD⁺] ratios by blockade of one pathway.

We further investigated whether the altered hepatic cytosolic redox state is sufficient to enhance exercise capacities. To specifically lower the hepatic cytosolic [NADH]/[NAD⁺] ratio, we applied water-forming NADH oxidase from *Lactobacillus brevis* (LbNOX), which converts cytosolic NADH into NAD⁺ without affecting the mitochondrial redox state^{17,18}. Using an adenoviral system, we induced LbNOX selectively in C57BL/6J mouse livers (Ad-LbNOX mice), which reduced hepatic [lactate]/[pyruvate] ratios without significant changes in the whole-liver [NADH]/[NAD⁺] ratios (Extended Data Fig. 5a–e), as previously reported^{17,18}. Hepatic LbNOX expression minimally altered body compositions, liver glycogen contents and hepatic gluconeogenic enzyme expressions (Extended Data Fig. 5f–k). As expected, Ad-LbNOX mice exhibited higher blood glucose levels than control mice after administrations of redox-dependent substrates (lactate and glycerol) (Fig. 4a,f) but not redox-independent substrates (pyruvate, alanine and DHA) (Extended Data Fig. 5l–n). Notably, hepatic LbNOX expression markedly increased the capacities for exercise of both intensities (Fig. 4b,g). Hepatic LbNOX expression in C57BL/6N mice produced similar results (Extended Data Fig. 5o,p). Consistently, compared to control mice, Ad-LbNOX mice showed higher blood glucose with lower plasma lactate and similar plasma glycerol levels during high-intensity exercise or with lower plasma glycerol, and unchanged plasma lactate during low-intensity exercise (Fig. 4c–e,h–j). Therefore, decreased hepatic cytosolic [NADH]/[NAD⁺] ratios are sufficient to enhance capacities for exercise of both intensities.

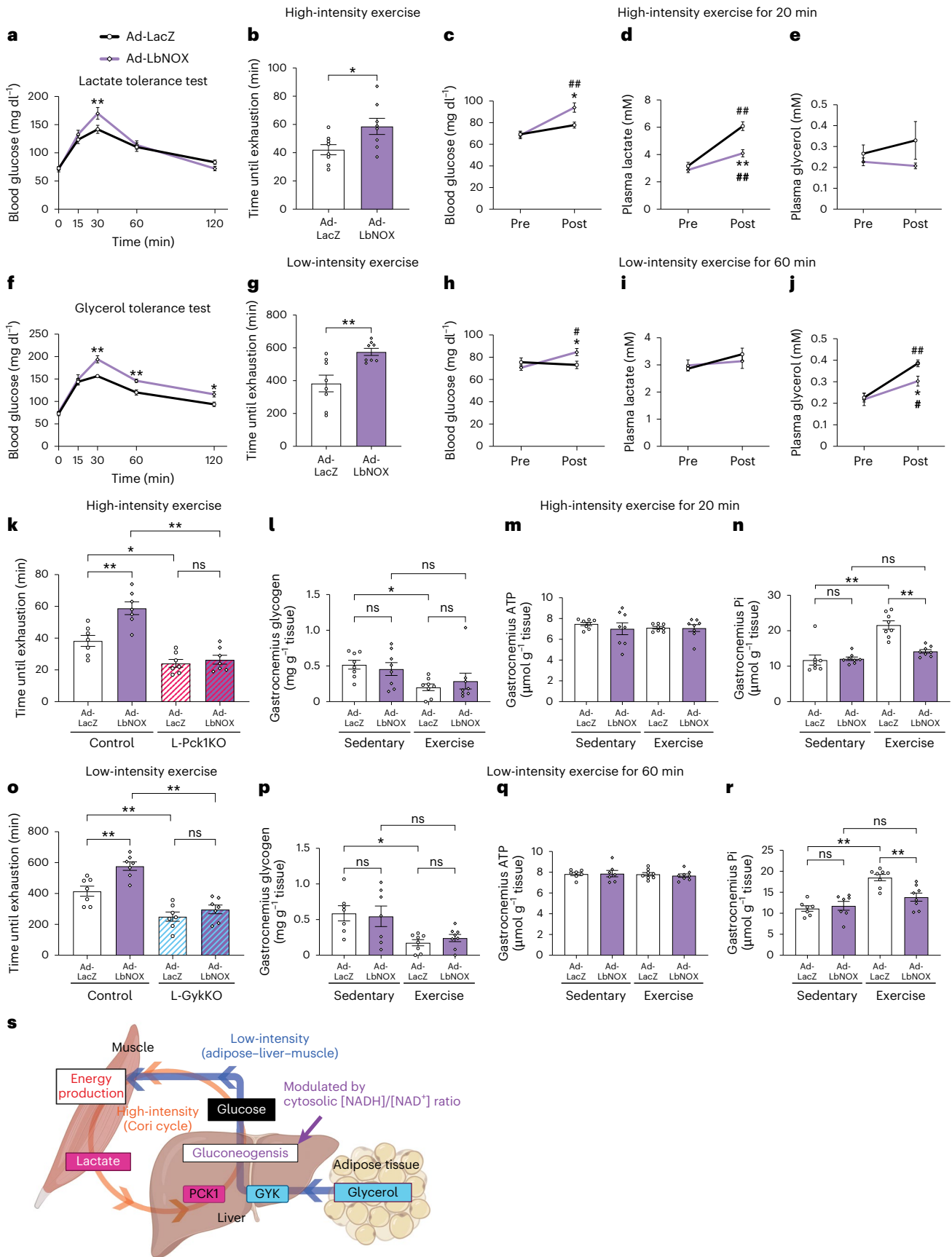
Given that NAD(H) is involved in numerous enzymatic reactions, we investigated whether the LbNOX-induced increases in exercise capacities are genuinely mediated by enhanced gluconeogenesis by examining the effects of hepatic LbNOX expression in combination with L-Pck1KO or L-GykKO. Most strikingly, the LbNOX-induced enhancements of high-intensity and low-intensity exercise capacities were almost completely blocked by L-Pck1KO and L-GykKO, respectively

(Fig. 4k,o). These results clearly indicate that enhanced exercise capacities in response to decreased hepatic cytosolic [NADH]/[NAD⁺] ratios are essentially attributable to enhanced gluconeogenesis from lactate and glycerol in high-intensity and low-intensity exercise, respectively. Similar results were obtained using female mice (Extended Data Fig. 5q,r). Furthermore, although most of our experiments were conducted on fasted animals to focus on gluconeogenesis, we obtained similar results even under ad libitum conditions (Extended Data Fig. 5s,t), probably because hepatic glycogen is depleted before exhaustion¹⁹. Therefore, gluconeogenesis is a potent determinant of exercise capacities, regardless of gender or feeding conditions. Hepatic cytosolic redox states modulate capacities for exercise with different intensities through two distinct hepatic gluconeogenic pathways.

We further examined muscle phenotypes under sedentary and exercised conditions. As exercise progresses, muscle glycogen content decreases, and ATP breakdown products, for example, inorganic phosphate (Pi), accumulate before ATP content decreases^{20–22}. Although muscle glycogen contents were reduced after exercise in the models with decreased exercise capacities (that is, L-Pck1KO mice with high-intensity exercise and L-GykKO mice with low-intensity exercise), the decrements in the models with increased exercise capacities (that is, L-Pck1KO mice with low-intensity exercise, L-GykKO mice with high-intensity exercise and LbNOX mice with exercise of both intensities) were not statistically significant (Fig. 4l,p and Extended Data Fig. 6a–d). Muscle ATP levels were similar to those in sedentary mice, except for decreased ATP levels in L-Pck1KO mouse muscles after high-intensity exercise, suggesting their near-complete exhaustion (Fig. 4m,q and Extended Data Fig. 6e–h). Notably, post-exercise accumulation of muscle Pi was larger in the models with decreased exercise capacities than in the corresponding controls (Extended Data Fig. 6i,j). By contrast, there was less muscle Pi accumulation in the models with increased exercise capacities than in the corresponding controls (Fig. 4n,r and Extended Data Fig. 6k,l). Longitudinal training reportedly induces muscle adaptations, such as increases in muscle glycogen content, fatty acid oxidation and mitochondrial electron transport chain-related enzymes^{23–25}. On the other hand, except for the upregulated fatty acid transporter *Cd36* in L-Pck1KO mice during low-intensity exercise, enzymes related to fatty acid oxidation and mitochondrial electron transport chain were unchanged (Extended Data Fig. 7a–f). Collectively, these findings indicate that altered gluconeogenesis has profound impacts on muscle ATP production under exercised, but not sedentary, conditions.

Fig. 4 | Hepatic LbNOX expression enhances capacities for exercise of both intensities by enhanced redox-dependent gluconeogenesis. a,f, Blood glucose levels of Ad-LacZ and Ad-LbNOX mice after intraperitoneal administrations of lactate (a) and glycerol (f). *n* = 8 (in a) and *n* = 7 (in f) per group; repeated measures two-way ANOVA followed by Holm–Šidák post hoc analysis (two-sided); ***P* < 0.0001 vs Ad-LacZ (at 30 min) (in a); ***P* = 0.0003 vs Ad-LacZ (at 30 min), ***P* = 0.0097 vs Ad-LacZ (at 60 min), ***P* = 0.0257 vs Ad-LacZ (at 120 min) (in f). b,g, Exercise capacities for high-intensity (b) and low-intensity (g) exercise in male Ad-LacZ and Ad-LbNOX mice were determined based on the times until exhaustion. *n* = 8 per group; two-tailed unpaired *t*-test; **P* = 0.0284 (in b); ***P* = 0.0037 (in g). c–e,h–j Concentrations of blood glucose (c,h), plasma lactate (d,i) and plasma glycerol (e,j) in male Ad-LacZ and Ad-LbNOX mice were measured before and after 20 min of high-intensity exercise or 60 min of low-intensity exercise. *n* = 8 per group; repeated measures two-way ANOVA followed by Holm–Šidák post hoc analysis (two-sided); **P* = 0.0391 vs control (post), #*P* = 0.0050 vs pre (within Ad-LbNOX) (in c); ***P* < 0.0001 vs Ad-LacZ (post), ##*P* < 0.0001 vs pre (within both groups) (in d). k,o, Male control and L-Pck1KO or L-GykKO mice were intravenously administered adenovirus vector expressing LacZ or LbNOX, as indicated, 1 week after tamoxifen treatment. Then, 1 week after the adenovirus injection, mice were subjected to high-intensity (k) or low-intensity (o) exercise and their times until exhaustion were recorded. *n* = 7 per group; one-way ANOVA followed by Tukey's post hoc analysis (two-sided); ***P* = 0.0008 for Ad-LacZ vs Ad-LbNOX (within control), **P* = 0.0240

for control vs L-Pck1KO (within Ad-LacZ), ***P* < 0.0001 for control vs L-Pck1KO (within Ad-LbNOX) (in k); ***P* = 0.0037 for Ad-LacZ vs Ad-LbNOX (within control), ***P* = 0.0033 for control vs L-GykKO (within Ad-LacZ), ***P* < 0.0001 for control vs L-GykKO (within Ad-LbNOX) (in o). l–n,p–r, Contents of glycogen (l,n), ATP (m,q) and Pi (n,r) in the gastrocnemius were measured in male Ad-LacZ and Ad-LbNOX mice under sedentary conditions and with the indicated intensity of exercise. *n* = 8 per group (in l–n); *n* = 7 per group in sedentary, *n* = 8 per group in exercise (in p–q); one-way ANOVA followed by Tukey's post hoc analysis (two-sided); **P* = 0.0479 for sedentary vs exercise (within Ad-LacZ) (in l); ***P* < 0.0001 for sedentary vs exercise (within Ad-LacZ), ***P* < 0.0001 for Ad-LacZ vs Ad-LbNOX (within exercise) (in n); **P* = 0.0170 for sedentary vs exercise (within LacZ) (in p); ***P* < 0.0001 for sedentary vs exercise (within LacZ), ***P* = 0.0031 for Ad-LacZ vs Ad-LbNOX (within exercise) (in r). s, Summary of the inter-organ networks during high-intensity and low-intensity exercise. In high-intensity exercise, cross-talk between muscle and liver mediated by lactate-derived gluconeogenesis has a key role in energy production. In low-intensity exercise, the inter-organ network between adipose–liver–muscle by glycerol-derived gluconeogenesis is important for energy production. The liver serves as a hub linking these inter-organ networks, wherein the hepatic cytosolic [NADH]/[NAD⁺] ratio modulates gluconeogenesis from lactate or glycerol. The schematic diagram was created in BioRender.com. Experiments shown in a, b, c–e, f, g, h–j, k, l–n, o and p–r were conducted using distinct cohorts of biologically independent mice. All data are presented as means; error bars, s.e.m. Each plot on the bar graph shows raw data.



In this study, we have shown that hepatic gluconeogenesis utilizing lactate and glycerol has primary roles in muscle ATP production during high-intensity and low-intensity exercise, respectively. Lactate is rapidly produced by muscle glycolysis and thereby acutely reaches its high blood concentrations²⁶, matching high-intensity exercise requiring large amounts of glucose production within a short time period. On the other hand, glycerol appears to be suitable for prolonged periods of low-intensity exercise, considering its abundant storage in adipose tissue²⁷. Our findings provide insights into the mechanism(s) underlying exercise-induced upregulation of gluconeogenesis: differential increases in gluconeogenic substrate supplies, rather than changes in the expressions of gluconeogenic enzymes, trigger enhanced gluconeogenesis during exercise. In contrast to transcriptional changes with relatively slow and lasting effects, the regulatory mechanism involving the supply of substrates appears to be a system that enables appropriately flexible adjustments to rapidly changing energy demands during exercise. Therefore, the shift of the major gluconeogenic substrate supply, in linkage with distinct hepatic pathways, achieves prompt metabolic adaptations to exercise of different intensities.

Our liver-specific manipulations of gluconeogenesis had minimal effects on enzyme expressions in muscle. From a systemic perspective, cross-talk between muscle and liver through the lactate–glucose carbon recycling system, known as the Cori cycle²⁶, modulates high-intensity exercise capacity. In line with our results, liver-specific knockout of both mitochondrial pyruvate carrier 2 and alanine transaminase 2, which impaired PCK1-mediated gluconeogenesis, was reported to decrease exercise capacities with lower blood glucose levels and increased blood lactate levels²⁸. Furthermore, upregulated lactate-derived gluconeogenesis in liver-specific prolyl hydroxylase 2 knockout mice reportedly enhanced high-intensity exercise performance²⁹. In addition to the classically recognized importance of the Cori cycle in high-intensity exercise²⁶, our findings demonstrate that for low-intensity exercise, the adipose–liver–muscle connection mediated by glycerol-derived gluconeogenesis is vital. Viewed collectively, our present results illustrate the important concept that the liver serves as a hub in the inter-organ network, which maintains energy metabolism during exercise through differentially regulated gluconeogenesis utilizing individual redox-dependent substrates (Fig. 4s).

Although fatty acids are known to be a major fuel source for muscle^{1,30}, glucose metabolism is considered to greatly affect exercise capacities in our models with hepatic deficiencies of gluconeogenic enzymes. Additionally, considering that mice reportedly rely more heavily on gluconeogenesis for circulating glucose than humans do³⁰, the contributions of gluconeogenesis to muscle ATP production might vary among species. Further studies are required to comprehensively elucidate the details of metabolism during exercise and demonstrate its applicability to human exercise.

As evidenced by the isotopic flux analysis, the reciprocally increased exercise capacities were attributable to enhanced gluconeogenesis from glycerol and lactate in L-Pck1KO and L-GykKO mice, respectively. Although a previous study examined the intrahepatic metabolic flux during exercise in congenital liver-specific PCK1 knockout mice with diet-induced obesity³¹, we demonstrate here that redox-dependent gluconeogenesis is differentially enhanced according to exercise intensities, thereby modulating exercise capacities. We have further shown that the hepatic cytosolic [NADH]/[NAD⁺] ratio is crucial for determining capacities for gluconeogenesis from redox-dependent substrates. Interestingly, hepatic PCK1/GYK deletion reduces the cytosolic [NADH]/[NAD⁺] ratio, probably by blockage of the flux of lactate-derived or glycerol-derived gluconeogenesis that consumes cytosolic NAD⁺, which in turn enhances gluconeogenesis through the alternative unblocked redox-dependent pathway. This mechanism may have risk-hedging roles in preventing hypoglycaemia by compensatory augmentation of the alternative gluconeogenic pathway, even if one

pathway is impaired. Furthermore, experiments with LbNOX revealed that decreased hepatic cytosolic [NADH]/[NAD⁺] ratios are sufficient to increase exercise capacities through the promotion of gluconeogenesis. In particular, gluconeogenesis was enhanced specifically under conditions with excessive supplies of redox-dependent substrates (that is, during lactate or glycerol tolerance tests and high-intensity or low-intensity exercise) but not under stable conditions (that is, in sedentary states). Thus, this system may function exclusively in response to upregulated redox-dependent substrate supplies, thereby avoiding resting hyperglycaemia. Recent studies have demonstrated that the liver is a bottleneck in metabolic flux during exercise, seemingly because of gluconeogenesis-induced cataplerotic stress; that is, the loss of TCA cycle intermediates^{30,32}. Therefore, decreasing hepatic cytosolic [NADH]/[NAD⁺] ratios, which replenish the intermediates by enhancing the influx of redox-dependent substrates, may achieve more efficient metabolic flow of the TCA cycle during exercise.

Methodologies to promote exercise performance have been attracting attention from the viewpoints of both sports and healthier lifestyle interventions^{33–35}. Regarding the applicability of our findings to promoting exercise performance, decreasing the hepatic cytosolic [NADH]/[NAD⁺] ratio might be a beneficial approach to enhancing exercise capacities regardless of their intensities. Although 4–8 weeks of endurance training reportedly increased the exercise capacities of C57BL/6 mice by approximately 10–30%^{36–39}, hepatic LbNOX expression prolonged exercise durations by 39% and 50% in high-intensity and low-intensity exercise, respectively. Therefore, regulating hepatic cytosolic redox appears to impact exercise capacities, presumably beyond the improvement achieved by long-term training. The liver cytosolic redox state is a promising target for enhancing exercise performance.

Methods

Ethics statement

All animal experiments were conducted in accordance with the Tohoku University institutional guidelines. Ethics approval was obtained from the Institutional Animal Care and Use Committee of the Tohoku University Environmental and Safety Committee.

Generation of *Pck1*-floxed mouse

To generate *Pck1*-floxed mice for the conditional knockout, two loxP sequences were inserted into the mouse *Pck1* gene locus by homology-dependent repair in mouse zygotes using CRISPR–Cas9 genome editing (Extended Data Fig. 8a). The *Pck1*-floxed mice were generated at the University of Tsukuba (Ibaraki, Japan). All mouse experiments were approved by the University of Tsukuba Animal Experiment Committee. Two mouse genomic sequences (5'-TAGCTGTAGCTATGGTCCG-3' and 5'-AAGGTCTGGGAAGCGCGTA-3') in introns 3 and 5, respectively, of *Pck1* were selected as guide RNA (gRNA) targets. Each sequence was inserted into a *pX330-mC* plasmid, which carried both the gRNA and Cas9 expression units⁴⁰. The flox donor plasmid DNA, *pflox-Pck1*, carried the genomic region from 907 bp upstream from exon 1 to 220 bp downstream from exon 6 of *Pck1*. Two loxP sequences were inserted at 286 bp upstream from exon 4 and 270 bp downstream from exon 5 in this donor vector. The aforementioned DNA vectors were isolated with a FastGene Plasmid Mini Kit (Nippon Genetics) and filtered with a MILLEX-GV 0.22 µm Filter unit (Merk Millipore) for microinjection. Pregnant mare serum gonadotropin (five units) and human chorionic gonadotropin (five units) were intraperitoneally injected into female C57BL/6J mice with a 48 h interval, followed by mating with male C57BL/6J mice. The zygotes from oviducts in mated females were collected, and mixtures of both *pX330-mC* (circular, 5 ng µl⁻¹ each) and *pflox-Pck1* (circular, 10 ng µl⁻¹) were microinjected into the zygotes. Subsequently, surviving injected zygotes were transferred into the oviducts of pseudo-pregnant ICR females and newborns were thereby obtained. To confirm the intended flox mutation, the genomic DNA was purified from the tails of G0 mice

with PI-200 (Kurabo Industries) according to the manufacturer's protocol. Genomic PCR was performed with KOD-Fx (TOYOBO). The primers (P_{Pck1-F} : 5'-GGCTCGCAGAGAAGTCTTTACAACCTGTG-3' and P_{Pck1-R} : 5'-CAGCAAGTGCCTTTACCCATAGACTTGT-3') were used for confirmation of the correct flox and large deletion mutations. In addition, random integrations of *pX330-mC* and *plox-Pck1* were checked by PCR with an ampicillin resistance gene detecting primer (P_{Amp-F} : 5'-TTGCCGGGAAGCTAGAGTAA-3' and P_{Amp-R} : 5'-TTTGCCTTCTGTTTTTGT-3').

Generation of *Gyk*-floxed mice

To generate *Gyk*-floxed mice for the conditional knockout, two loxP sequences were inserted into the mouse *Gyk* gene locus by homology-dependent repair in embryonic stem cells using CRISPR-Cas9 genome editing (Extended Data Fig. 8b). Generation of the *Gyk*-floxed mice was performed at Trans Genic (Fukuoka, Japan) with institutional Animal Research Committee approval. To construct the donor vector to insert the two lox sequences, a 2.1 kb mouse genomic fragment containing a part of intron 1 for the 5' homologous arm, a 2.2 kb fragment containing a part of intron 1, exon 2, intron 2, exon 3 and a part of intron 3 for the floxed region and a 2.2 kb fragment containing a part of intron 3 were amplified by PCR using primers with the loxP sequence from RENKA embryonic stem cell genomic DNA⁴¹. These fragments were subcloned into plasmids, and the resulting donor vector contained a 2.1 kb 5' homologous arm, the first loxP site, a 2.2 kb floxed region including exons 2 and 3, the second loxP site and a 2.2 kb 3' homologous arm. Two mouse genomic sequences (5'-AGCGTATCGTTCCCAGACAT-3' and 5'-AGCGTATCGTTCCCAGACAT-3') in introns 1 and 3, respectively, of *Gyk* were selected as gRNA targets. Each gRNA sequence was synthesized as an oligonucleotide DNA, ligated with the U6 promoter and inserted into the plasmid containing the CAG promoter-driven hCas9 coding sequence to construct the expression vector. To validate the efficiency of the gene-targeted double-strand break using the designed sgRNA and hCas9, reconstitution of green fluorescence by homology-dependent repair of EGFP was examined⁴². The donor vector, two expression vectors and a plasmid containing the PGK-driven puromycin-resistant gene for transfectant selection were introduced into RENKA embryonic stem cells (C57BL/6N) by electroporation. After selection using puromycin, the resistant clones were isolated, and their DNA samples were screened for loxP insertion by PCR using the following primer sets: $P_{Gyk-5-F}$: 5'-CCCCCGCGGCCGCTGAGGTTCTCATAGTTACACATCC-3' and $P_{Gyk-5-R}$: 5'-AGGGGCTATGGGCCATAACTTCG-3' to screen for 5' loxP insertion, and $P_{Gyk-3-F}$: 5'-CCTAGTCTGCCGATCCATAACTTC-3' and $P_{Gyk-3-R}$: 5'-CTCGAGGTCGACTGTGTCTGAGTCTAGTCTGGTCTCC-3' to screen for 3' loxP insertion. PCR-positive embryonic stem clones were expanded, and isolated DNA samples were further analysed by PCR amplification followed by restriction enzyme digestion to examine whether the two loxP sites are on the same allele. The primer set used in this PCR was $P_{Gyk-5-F}$ and $P_{Gyk-3-R}$ to amplify from intron 1 to intron 3, including the loxP insertion sequence. Amplified fragments were digested with PspOMI, the recognition sequence of which was introduced with the 5' loxP sequence, and BamHI, the recognition sequence of which was introduced with the 3' loxP sequence. Clones that showed a band at the double-digested size were considered to have the two loxP sites in a single allele (floxed allele). The insertion of loxP sites at the expected region was also confirmed by direct sequencing. Recombinant embryonic stem cell clones with the floxed region were also analysed by genomic Southern hybridization probed with the genomic sequence of the floxed region to confirm that these clones did not contain random integration of the donor vector. Recombinant embryonic stem cell clones with the floxed allele were aggregated with ICR eight-cell stage embryos to generate chimeric mice. Germline-transmitting F1 heterozygous mice were obtained by crossing chimeric mice with a high contribution of the RENKA embryonic

stem cells and C57BL/6N mice. The targeted allele was identified by PCR using primer sets $P_{Gyk-5-F}$ - $P_{Gyk-5-R}$ and $P_{Gyk-3-F}$ - $P_{Gyk-3-R}$, genomic Southern hybridization and direct sequencing in F1 mice.

Animals

All mice were group-housed in a plastic cage with a 12 h light, 12 h dark cycle and received a normal chow diet (MF Diet, cat. no. MF, Oriental Yeast) ad libitum. C57BL6/J or C57BL6/N mice were obtained from CLEA Japan. To obtain tamoxifen-inducible liver-specific knockout mice, we used transgenic mice expressing a Cre recombinase transgene fused to mutated estrogen receptor ligand-binding domains under the control of the serum albumin promoter (SA-CreER^{T2} mice)^{43,44}. To generate tamoxifen-inducible liver-specific PCK1 knockout mice (L-Pck1KO mice), we crossed SA-CreER^{T2} mice and *Pck1*-floxed mice. SA-CreER^{T2} -/-; *Pck1*-floxed mice (control mice) and SA-CreER^{T2} +/-; *Pck1*-floxed mice (L-Pck1KO mice) were used for experiments. To generate tamoxifen-inducible liver-specific GYK knockout mice (L-GykKO mice), we crossed SA-CreER^{T2} mice and *Gyk*-floxed mice. SA-CreER^{T2} -/-; *Gyk*-floxed mice (control mice) and SA-CreER^{T2} +/-; *Gyk*-floxed mice (L-GykKO mice) were used for experiments. To induce a knockout, mice were intraperitoneally administered 1 mg of tamoxifen for three consecutive days, 1 week before the experiments. All experiments were conducted using male mice at 16–18 weeks of age unless otherwise indicated. Experiments were performed under 24 h fasted conditions, at which point liver glycogen is almost entirely depleted except as otherwise provided. For measurements of liver metabolites, mice were anaesthetized with 2.5–3% isoflurane, and the liver was rapidly frozen by freeze-clamp within a few seconds after removal to avoid degradation of metabolites^{12,45,46}. Other organs were frozen in liquid nitrogen immediately after removal. For measurements of muscle metabolites during the exercise experiments, mice were killed by cervical dislocation, and the sampled gastrocnemius was rapidly frozen in liquid nitrogen.

Exercise experiments

A motorized treadmill (MK680, Muromachi Kikai) was used for all exercise experiments. Before the exercise experiments, mice were adapted to running on a treadmill at the indicated speed for six and three consecutive days before high-intensity and low-intensity exercise, respectively. The detailed protocols are shown in Supplementary Table 1. All pre-adaptations were conducted during the dark cycle. The exercise experiments started at 09:00 h (1 h after the onset of the dark cycle). In the high-intensity exercise protocol, mice started to run at 10 m min⁻¹, and the speed was increased incrementally by 1 m min⁻¹ every 1 min up to 25 m min⁻¹; the mice then ran until exhaustion or for 20 min. With the low-intensity exercise protocol, mice ran at 13 m min⁻¹ until exhaustion or for 60 min. The sedentary group of mice were placed on the treadmill machine without running (at 0 m min⁻¹) for the same period of time as the exercised mice. Exhaustion was defined as the inability to continue running with the mouse staying in the electrical shock grid for five consecutive seconds.

Isotopic metabolic flux analysis during exercise

Mice were treated with tamoxifen and adapted to treadmill running as above for 2 weeks before the exercise experiment. Catheters (CI0PU-MCA1301, Instech Laboratories) were implanted in the left common carotid artery for blood sampling and the right jugular vein for isotope infusion 1 week before the experiment, as previously reported⁴⁷. The free ends of catheters were plugged by PinPorts (PNP3F22, Instech Laboratories) after tunnelling under the skin to the back of the neck. Mice with a weight loss of over 10% on the experimental day compared with the pre-surgery weight were excluded. Food was removed 24 h before exercise. After placing the mice on the treadmill, blood was collected (t_0). Then, primed constant infusions of stable isotopes were started 210 min before exercise as previously reported³¹. For the

low-intensity exercise experiment on L-Pck1KO and their controls, [6,6-²H₂]glucose (priming with 400 μmol kg⁻¹ prime followed by continuous infusion of 40 μmol kg⁻¹ min⁻¹) (661414, Sigma-Aldrich) and [¹³C₃] glycerol (priming with 40 μmol kg⁻¹ followed by continuous infusion of 4 μmol kg⁻¹ min⁻¹) (CLM-1510-0, Cambridge Isotope Laboratories) were infused. For the high-intensity exercise experiment on L-GykKO and their controls, [6,6-²H₂]glucose (priming with 400 μmol kg⁻¹ for the prime infusion followed by continuous infusion of 40 μmol kg⁻¹ min⁻¹) and [¹³C₃] lactate (priming with 150 μmol kg⁻¹ followed by continuous infusion of 15 μmol kg⁻¹ min⁻¹) (746258, Sigma-Aldrich) were infused. Under the sedentary conditions, blood samples were collected at two different timepoints of approximately 20 min and 10 min before exercise and then recorded as *t*₁ and *t*₂, respectively. Blood samples were also collected during exercise. The timepoints were approximately 20 min (*t*₃) and 25 min (*t*₄) after starting high-intensity exercise or about 60 min (*t*₃) and 70 min (*t*₄) after starting low-intensity exercise. Plasma samples were collected after centrifugations of blood samples and stored at -80°C.

Sample analysis and calculations for metabolic flux

The concentration (*C*) and isotopic enrichment (IE) of glucose at each timepoint were measured using ion chromatography coupled with high-resolution mass spectrometry. An Orbitrap mass spectrometer (Q-Exactive Focus) and a high-performance ion chromatography system (ICS-5000+) enabled sensitive and selective detection based on anion separation and accurate mass measurement⁴⁸. IE at each timepoint was corrected by subtracting naturally occurring isotopes (IE at *t*₀ = IE₀). The glucose rate of appearance (Ra) was calculated using Steel's non-steady-state equation modified for stable-isotope experiments^{8,49},

$$\text{Glucose Ra} = \frac{F - V((C_m + C_n)/2)((IE_n - IE_m)/(t_n - t_m))}{(IE_m + IE_n)/2}$$

where *F* is the infusion rate of [6,6-²H₂]glucose (40 μmol kg⁻¹ min⁻¹) and *V* is the volume of distribution, which was assumed to be 40 ml kg⁻¹. Glucose rate of appearance was calculated using IE for [6,6-²H₂]glucose. Values at *t*₁ and *t*₂ (*m* = 1 and *n* = 2) were used to obtain the metabolic flux rates under sedentary conditions, while metabolic flux rates during exercise were calculated using values at *t*₃ and *t*₄ (*m* = 3 and *n* = 4). The contents of ¹³C-labelled glucose were calculated as the average ratio to [¹²C₆]glucose at *t*₃ and *t*₄.

RNA purification and quantitative PCR with reverse transcription

Using the RNeasy mini kit (Qiagen), total RNA was extracted from mouse liver or gastrocnemius, which had been stored in RNAlater Tissue Reagent (Qiagen). Complementary DNA, synthesized from 1 μg of total RNA using a ReverTra Ace qPCR RT Master Mix (TOYOBO), was evaluated with a CFX96 Touch Real-Time PCR Detection System (Bio-Rad). mRNA expression levels were normalized to the levels of *hydroxymethylbilane synthase* (*Hmbs*) in the liver and *glyceraldehyde-3-phosphate dehydrogenase* (*Gapdh*) in gastrocnemius. The sequences of the primers are listed in Supplementary Table 2.

Western blotting analysis

Mouse tissues were homogenized in lysis buffer (100 mM Tris pH 8.5, 250 mM NaCl, 1 mM EDTA, 1% NP-40) containing protease inhibitors (35 mg ml⁻¹ phenylmethylsulfonyl fluoride, 10 mg ml⁻¹ aprotinin and 10 mg ml⁻¹ leupeptin). After centrifugation at 20,400g for 5 min, the protein concentrations of supernatants were determined using a Pierce BCA Protein Assay Kit (Thermo Fisher Scientific). Equal amounts of proteins with Laemmli SDS sample buffer were boiled for 5 min. Next, 30 μg of tissue protein extracts were loaded onto an SDS-PAGE column and then transferred to a nitrocellulose membrane. After blocking with

Tris-buffered saline containing 2–5% skim milk, membranes were incubated with antibodies to GAPDH (S174S, Cell Signaling Technology), GYK (ab126599, Abcam), PCK1 (16754-1-AP, Proteintech), pyruvate carboxylase (16588-1-AP, Proteintech), fructose-1,6-bisphosphatase 1 (ab109732, Abcam) or FLAG (2368S, Cell Signaling Technology). After washing, the membranes were incubated with anti-rabbit horseradish peroxidase-linked IgG secondary antibody (NA9340V, GE HealthCare Japan). Chemiluminescence signal enhancement caused by the Pierce ECL Plus Western Blotting Substrate (Thermo Fisher Scientific) was detected with a ChemiDoc Touch Imaging System (Bio-Rad). Quantitative data were obtained using ImageJ software.

Tissue metabolite and blood analyses

Metabolites in the liver and gastrocnemius muscle extracts were measured after deproteinization with perchloric acid (26503-75, Nacalai Tesque). Blood samples were obtained from the tail vein. Liver and muscle glycogen levels were measured after amyloglucosidase digestion as previously described^{50,51}. Commercial kits were used for measuring lactate (K607, BioVision), pyruvate (K609, BioVision), alanine (MET-5093, Cell Biolabs), free fatty acids (279-75401, FUJIFILM Wako), ketone bodies (ab272541, Abcam), NAD(H) (N509, Dojindo), ATP (ab83355, Abcam) and Pi (ab65622, Abcam) according to the relevant instructions for each.

Tolerance tests of gluconeogenic substrates

Mice were intraperitoneally administered 1 g kg⁻¹ body weight of gluconeogenic substrates diluted in PBS. The substrates were glycerol (075-00611, FUJIFILM Wako), DHA (NA-0183, Combi-Blocks), lactate (L7022, Sigma-Aldrich), pyruvate (P8574, Sigma-Aldrich) and alanine (010-01042, FUJIFILM Wako). Glucose levels in blood from the tail vein were measured using a Glutestmint Kit (Sanwa Kagaku Kenkyusho) before and 15, 30, 60 and 120 min after injections of the substrates.

Primary hepatocyte experiments

Primary hepatocytes were isolated by perfusion and digestion using Liberase (Roche) as previously reported⁵². Dead cells were removed using Percoll (17-0891-01, GE HealthCare Japan). Isolated hepatocytes were seeded at 10⁵ cells per well into 12-well collagen-coated dishes in DMEM (11995065, Thermo Fisher Scientific) supplemented with 10% FBS, 1% penicillin–streptomycin, 10 mM HEPES, 1 nM dexamethasone and 0.5 U ml⁻¹ insulin. After overnight incubation at 37°C in a 5% CO₂ chamber, cells were washed three times with PBS, followed by a 2 h incubation in no-glucose DMEM (1443001) supplemented with 10 mM HEPES. After the cells had been washed three times with PBS, they were incubated for 3 h in 10 mM HEPES no-glucose DMEM containing 10 mM glycerol or lactate with or without 10 mM ethanol. Glucose levels in media were measured with normalization to total protein concentrations from hepatocytes lysed in 1% SDS and expressed as a percentage of the glucose amount produced in the absence of a substrate.

Adenovirus experiments

FLAG-tagged LbNOX was generated with a ViraPower Adenoviral Expression Kit (K493000, Thermo Fisher Scientific) using a subcloned gene from pUC57-LbNOX. pUC57-LbNOX was a gift from V. Mootha (Addgene, plasmid 75285; http://n2t.net/addgene:75285;RRID:Addgene_75285)¹⁷. LacZ adenovirus was used as a control. Adenovirus (1 × 10⁹ plaque-forming units) was intravenously injected into 16-week-old wild-type C57BL/6J mice, C57BL/6N mice or knockout mice and the corresponding controls 1 week after tamoxifen treatment.

Statistics and reproducibility

No statistical method was used to predetermine sample size. However, the sample sizes used in this study are consistent with those in previous publications^{9,29,31} and were considered sufficient based on our prior experience with similar experimental designs^{44,53}. Mice with abnormal

body weights were excluded before the experiments. In the isotopic flux analysis (Fig. 2i–m), mice with >10% weight loss on the day of the experiment (compared to pre-surgery weight) or with technical failures (for example, catheter withdrawal) were excluded. In Extended Data Fig. 2m, one epididymal white adipose tissue weight measurement was missing in the L-GykKO group and was therefore excluded. No other data points were excluded. Animals were randomly assigned to experimental groups after matching for body weight. Data collection and analysis were not performed blind to the conditions of the experiments.

Data distribution was assumed to be normal, but this was not formally tested. All statistical tests were two-sided. For comparisons between two groups, two-tailed unpaired *t*-tests were used. For comparisons involving more than two groups without a time component (that is, bar graphs), one-way ANOVA followed by Tukey's post hoc analysis was performed. For time-course experiments (that is, line graphs), repeated measures two-way ANOVA was used when all groups had the same number of samples (balanced design), and a mixed-effects model based on restricted maximum likelihood was used when group sizes differed (unbalanced design). In both cases, Holm–Šidák post hoc analyses were applied for multiple comparisons. For Holm–Šidák analyses, comparisons were restricted to predefined relevant comparisons; specifically, within-timepoint comparisons between genotypes or treatment groups (for example, control vs KO or Ad-LacZ vs Ad-LbNOX at each timepoint), and within-group comparisons across time (for example, pre vs post within control or KO). Cross-group timepoint comparisons (for example, pre-control vs post-KO) were not conducted. In cases for which no significant main effects or interactions were detected by ANOVA or mixed-effects models, post hoc analysis was not performed. Data are presented as means ± s.e.m. Each plot on the bar graph shows raw data. *P* values are denoted in figures as not significant (ns), **P* < 0.05 or ***P* < 0.01. Exact *P* values and sample sizes (*n*) for each group are provided in the figure legends. Prism 10 (GraphPad Software) was used for all statistical analyses.

Reporting summary

Further information on research design is available in the Nature Portfolio Reporting Summary linked to this article.

Data availability

No datasets were generated or analysed during the current study. Source data are provided with this paper.

References

- Hargreaves, M. & Spriet, L. L. Skeletal muscle energy metabolism during exercise. *Nat. Metab.* **2**, 817–828 (2020).
- Trefts, E., Williams, A. S. & Wasserman, D. H. Exercise and the regulation of hepatic metabolism. *Prog. Mol. Biol. Transl. Sci.* **135**, 203–225 (2015).
- Petersen, M. C., Vatner, D. F. & Shulman, G. I. Regulation of hepatic glucose metabolism in health and disease. *Nat. Rev. Endocrinol.* **13**, 572–587 (2017).
- Zhang, X., Yang, S., Chen, J. & Su, Z. Unraveling the regulation of hepatic gluconeogenesis. *Front. Endocrinol. (Lausanne)* **9**, 802 (2018).
- Egan, B. & Zierath, J. R. Exercise metabolism and the molecular regulation of skeletal muscle adaptation. *Cell Metab.* **17**, 162–184 (2013).
- Gaitanos, G. C., Williams, C., Boobis, L. H. & Brooks, S. Human muscle metabolism during intermittent maximal exercise. *J. Appl. Physiol. (1985)* **75**, 712–719 (1993).
- Brooks, G. A. The precious few grams of glucose during exercise. *Int. J. Mol. Sci.* **21**, 5733 (2020).
- Romijn, J. A. et al. Regulation of endogenous fat and carbohydrate metabolism in relation to exercise intensity and duration. *Am. J. Physiol.* **265**, E380–E391 (1993).
- Okamoto, M. et al. Hormetic effects by exercise on hippocampal neurogenesis with glucocorticoid signaling. *Brain Plast.* **1**, 149–158 (2015).
- She, P. et al. Phosphoenolpyruvate carboxykinase is necessary for the integration of hepatic energy metabolism. *Mol. Cell. Biol.* **20**, 6508–6517 (2000).
- Williamson, D. H., Lund, P. & Krebs, H. A. The redox state of free nicotinamide-adenine dinucleotide in the cytoplasm and mitochondria of rat liver. *Biochem. J.* **103**, 514–527 (1967).
- Madiraju, A. K. et al. Metformin inhibits gluconeogenesis via a redox-dependent mechanism in vivo. *Nat. Med.* **24**, 1384–1394 (2018).
- Madiraju, A. K. et al. Metformin suppresses gluconeogenesis by inhibiting mitochondrial glycerophosphate dehydrogenase. *Nature* **510**, 542–546 (2014).
- Krebs, H. A. & Gascoyne, T. The redox state of the nicotinamide-adenine dinucleotides in rat liver homogenates. *Biochem. J.* **108**, 513–520 (1968).
- Krebs, H. A., Freedland, R. A., Hems, R. & Stubbs, M. Inhibition of hepatic gluconeogenesis by ethanol. *Biochem. J.* **112**, 117–124 (1969).
- Mezey, E. Metabolic effects of alcohol. *Fed. Proc.* **44**, 134–138 (1985).
- Titov, D. V. et al. Complementation of mitochondrial electron transport chain by manipulation of the NAD⁺/NADH ratio. *Science* **352**, 231–235 (2016).
- Goodman, R. P. et al. Hepatic NADH reductive stress underlies common variation in metabolic traits. *Nature* **583**, 122–126 (2020).
- López-Soldado, I., Guinovart, J. J. & Duran, J. Increased liver glycogen levels enhance exercise capacity in mice. *J. Biol. Chem.* **297**, 100976 (2021).
- Kent-Braun, J. A., Fitts, R. H. & Christie, A. Skeletal muscle fatigue. *Compr. Physiol.* **2**, 997–1044 (2012).
- Allen, D. G., Lamb, G. D. & Westerblad, H. Skeletal muscle fatigue: cellular mechanisms. *Physiol. Rev.* **88**, 287–332 (2008).
- Lewsey, S. C. et al. Exercise intolerance and rapid skeletal muscle energetic decline in human age-associated frailty. *JCI Insight* **5**, e141246 (2020).
- Fuller, S. E. et al. Low-intensity exercise induces acute shifts in liver and skeletal muscle substrate metabolism but not chronic adaptations in tissue oxidative capacity. *J. Appl. Physiol. (1985)* **127**, 143–156 (2019).
- Matsumoto, J. et al. Brain-derived neurotrophic factor improves impaired fatty acid oxidation via the activation of adenosine monophosphate-activated protein kinase-α-proliferator-activated receptor-γ coactivator-1α signaling in skeletal muscle of mice with heart failure. *Circ. Heart Fail.* **14**, e005890 (2021).
- Lundby, C. & Jacobs, R. A. Adaptations of skeletal muscle mitochondria to exercise training. *Exp. Physiol.* **101**, 17–22 (2016).
- Brooks, G. A. The science and translation of lactate shuttle theory. *Cell Metab.* **27**, 757–785 (2018).
- Langin, D. Control of fatty acid and glycerol release in adipose tissue lipolysis. *C. R. Biol.* **329**, 598–607 (2006).
- Martino, M. R. et al. Disruption of hepatic mitochondrial pyruvate and amino acid metabolism impairs gluconeogenesis and endurance exercise capacity in mice. *Am. J. Physiol. Endocrinol. Metab.* **326**, E515–E527 (2024).
- Suhara, T. et al. Inhibition of the oxygen sensor PHD2 in the liver improves survival in lactic acidosis by activating the Cori cycle. *Proc. Natl Acad. Sci. USA* **112**, 11642–11647 (2015).
- Axsom, J. et al. Quantification of nutrient fluxes during acute exercise in mice. *Cell Metab.* **36**, 2560–2579.e5 (2024).
- Rome, F. I. et al. Loss of hepatic phosphoenolpyruvate carboxykinase 1 dysregulates metabolic responses to acute exercise but enhances adaptations to exercise training in mice. *Am. J. Physiol. Endocrinol. Metab.* **324**, E9–E23 (2023).

32. Inigo, M., Deja, S. & Burgess, S. C. Ins and outs of the TCA cycle: the central role of anaplerosis. *Annu. Rev. Nutr.* **41**, 19–47 (2021).
33. Gremeaux, V. et al. Exercise and longevity. *Maturitas* **73**, 312–317 (2012).
34. Rueggsegger, G. N. & Booth, F. W. Health benefits of exercise. *Cold Spring Harb. Perspect. Med.* **8**, a029694 (2018).
35. Ketelhut, S. & Ketelhut, R. G. Type of exercise training and training methods. *Adv. Exp. Med. Biol.* **1228**, 25–43 (2020).
36. Abadi, A. et al. Supplementation with α -lipoic acid, CoQ10, and vitamin E augments running performance and mitochondrial function in female mice. *PLoS ONE* **8**, e60722 (2013).
37. Avila, J. J., Kim, S. K. & Massett, M. P. Differences in exercise capacity and responses to training in 24 inbred mouse strains. *Front. Physiol.* **8**, 974 (2017).
38. Fiuzza-Luces, C. et al. Muscle molecular adaptations to endurance exercise training are conditioned by glycogen availability: a proteomics-based analysis in the McArdle mouse model. *J. Physiol.* **596**, 1035–1061 (2018).
39. Massett, M. P., Matejka, C. & Kim, H. Systematic review and meta-analysis of endurance exercise training protocols for mice. *Front. Physiol.* **12**, 782695 (2021).
40. Mizuno-Iijima, S. et al. Efficient production of large deletion and gene fragment knock-in mice mediated by genome editing with Cas9-mouse Cdt1 in mouse zygotes. *Methods* **191**, 23–31 (2021).
41. Mishina, M. & Sakimura, K. Conditional gene targeting on the pure C57BL/6 genetic background. *Neurosci. Res.* **58**, 105–112 (2007).
42. Mashiko, D. et al. Generation of mutant mice by pronuclear injection of circular plasmid expressing Cas9 and single guided RNA. *Sci. Rep.* **3**, 3355 (2013).
43. Schuler, M., Dierich, A., Chambon, P. & Metzger, D. Efficient temporally controlled targeted somatic mutagenesis in hepatocytes of the mouse. *Genesis* **39**, 167–172 (2004).
44. Izumi, T. et al. Vagus–macrophage–hepatocyte link promotes post-injury liver regeneration and whole-body survival through hepatic FoxM1 activation. *Nat. Commun.* **9**, 5300 (2018).
45. Faupel, R. P., Seitz, H. J., Tarnowski, W., Thiemann, V. & Weiss, C. The problem of tissue sampling from experimental animals with respect to freezing technique, anoxia, stress and narcosis. A new method for sampling rat liver tissue and the physiological values of glycolytic intermediates and related compounds. *Arch. Biochem. Biophys.* **148**, 509–522 (1972).
46. Sugiura, Y. et al. Visualization of in vivo metabolic flows reveals accelerated utilization of glucose and lactate in penumbra of ischemic heart. *Sci. Rep.* **6**, 32361 (2016).
47. Sakai, G. et al. Effects of the activation of three major hepatic Akt substrates on glucose metabolism in male mice. *Endocrinology* **158**, 2659–2671 (2017).
48. Maeda, R. et al. Amino acid catabolite markers for early prognostication of pneumonia in patients with COVID-19. *Nat. Commun.* **14**, 8469 (2023).
49. Steele, R. Influences of glucose loading and of injected insulin on hepatic glucose output. *Ann. N. Y. Acad. Sci.* **82**, 420–430 (1959).
50. Penhoat, A., Fayard, L., Stefanutti, A., Mithieux, G. & Rajas, F. Intestinal gluconeogenesis is crucial to maintain a physiological fasting glycemia in the absence of hepatic glucose production in mice. *Metabolism* **63**, 104–111 (2014).
51. Kaneko, K. et al. The role of kidney in the inter-organ coordination of endogenous glucose production during fasting. *Mol. Metab.* **16**, 203–212 (2018).
52. Charni-Natan, M. & Goldstein, I. Protocol for primary mouse hepatocyte isolation. *STAR Protoc.* **1**, 100086 (2020).
53. Kawana, Y. et al. Optogenetic stimulation of vagal nerves for enhanced glucose-stimulated insulin secretion and β cell proliferation. *Nat. Biomed. Eng.* **8**, 808–822 (2024).

Acknowledgements

We thank T. Takasugi, K. Watanabe, T. Sueoka, Y. Akaogi, S. Goto, S. Komatsu, Y. Yoshizawa, M. Fukuda, M. Iwama, K. Takahashi and H. Yokoyama (all of whom belong to the Department of Diabetes, Metabolism and Endocrinology, Tohoku University Graduate School of Medicine) for technical support. This work was supported by Grants-in-Aid for Scientific Research to H.K. (20H05694) and to K.K. (22K08642) from the Japan Society for the Promotion of Science. This research was also supported by the Japan Science and Technology Agency (Moonshot Research & Development Program) (grant number JPMJMS2023 to H.K.). The funders had no role in study design, data collection and analysis, decision to publish or preparation of the paper.

Author contributions

T.H. and K.K. conducted the research and obtained the data, contributed to relevant discussions, wrote the paper and reviewed and edited the paper. S.H., K.U., S. Tomiyama, K.T., M.Y., A.E., H.S., Y.K., Y.A., S.K. and J.I. contributed to the relevant discussions. S.M. and S. Takahashi generated *Pck1*-floxed mice. A.T., H.O. and K.Y. contributed to mouse catheterization for the exercise flux analysis. R.M. and Y.S. conducted mass spectrometry analysis. H.K. contributed to the relevant discussions, writing of the paper and reviewing and editing of the paper.

Competing interests

The authors declare no competing interests.

Additional information

Extended data is available for this paper at <https://doi.org/10.1038/s42255-025-01373-z>.

Supplementary information The online version contains supplementary material available at <https://doi.org/10.1038/s42255-025-01373-z>.

Correspondence and requests for materials should be addressed to Keizo Kaneko or Hideki Katagiri.

Peer review information *Nature Metabolism* thanks Adam Rose, Xiaoyang Su and the other, anonymous, reviewer(s) for their contribution to the peer review of this work. Primary Handling Editors: Jean Nakhle and Ashley Castellanos-Jankiewicz, in collaboration with the *Nature Metabolism* team.

Reprints and permissions information is available at www.nature.com/reprints.

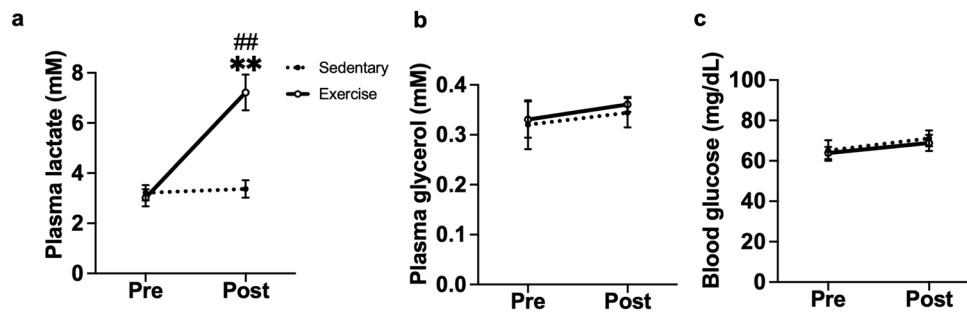
Publisher's note Springer Nature remains neutral with regard to jurisdictional claims in published maps and institutional affiliations.

Open Access This article is licensed under a Creative Commons Attribution 4.0 International License, which permits use, sharing, adaptation, distribution and reproduction in any medium or format, as long as you give appropriate credit to the original author(s) and the source, provide a link to the Creative Commons licence, and indicate if changes were made. The images or other third party material in this article are included in the article's Creative Commons licence, unless indicated otherwise in a credit line to the material. If material is not included in the article's Creative Commons licence and your intended use is not permitted by statutory regulation or exceeds the permitted use, you will need to obtain permission directly from the copyright holder. To view a copy of this licence, visit <http://creativecommons.org/licenses/by/4.0/>.

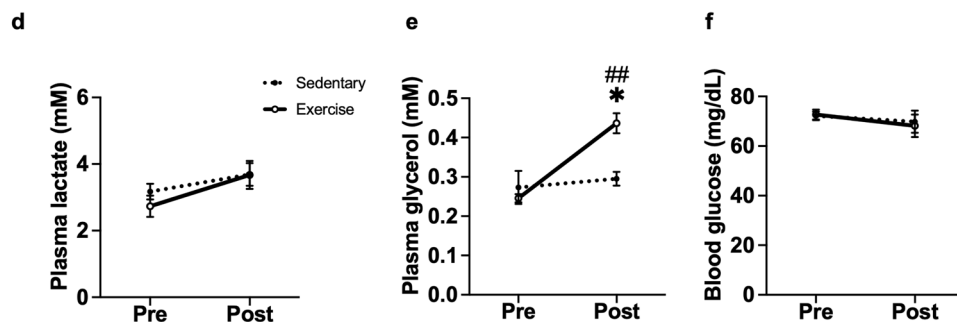
© The Author(s) 2025

¹Department of Diabetes, Metabolism and Endocrinology, Tohoku University Graduate School of Medicine, Sendai, Japan. ²Division of Endocrinology and Metabolism, Department of Internal Medicine, Teikyo University School of Medicine, Tokyo, Japan. ³SiRIUS Institute of Medical Research, Tohoku University, Sendai, Japan. ⁴Laboratory Animal Resource Center and Transborder Medical Research Center, Institute of Medicine, University of Tsukuba, Tsukuba, Japan. ⁵Department of Endocrinology, Hematology and Gerontology, Chiba University Graduate School of Medicine, Chiba, Japan. ⁶Department of Disease Prevention, Division of Clinical Preventive Medical Sciences, Center for Preventive Medical Sciences, Chiba University, Chiba, Japan. ⁷Chiba University, Chiba, Japan. ⁸Multomics Platform, Center for Cancer Immunotherapy and Immunobiology, Kyoto University Graduate School of Medicine, Kyoto, Japan. ⁹Human Biology Microbiome Quantum Research Center (WPI-Bio2Q), Keio University School of Medicine, Tokyo, Japan.
✉e-mail: kayzo@oak.dti.ne.jp; hideki.katagiri.e1@tohoku.ac.jp

High-intensity exercise for 20 minutes



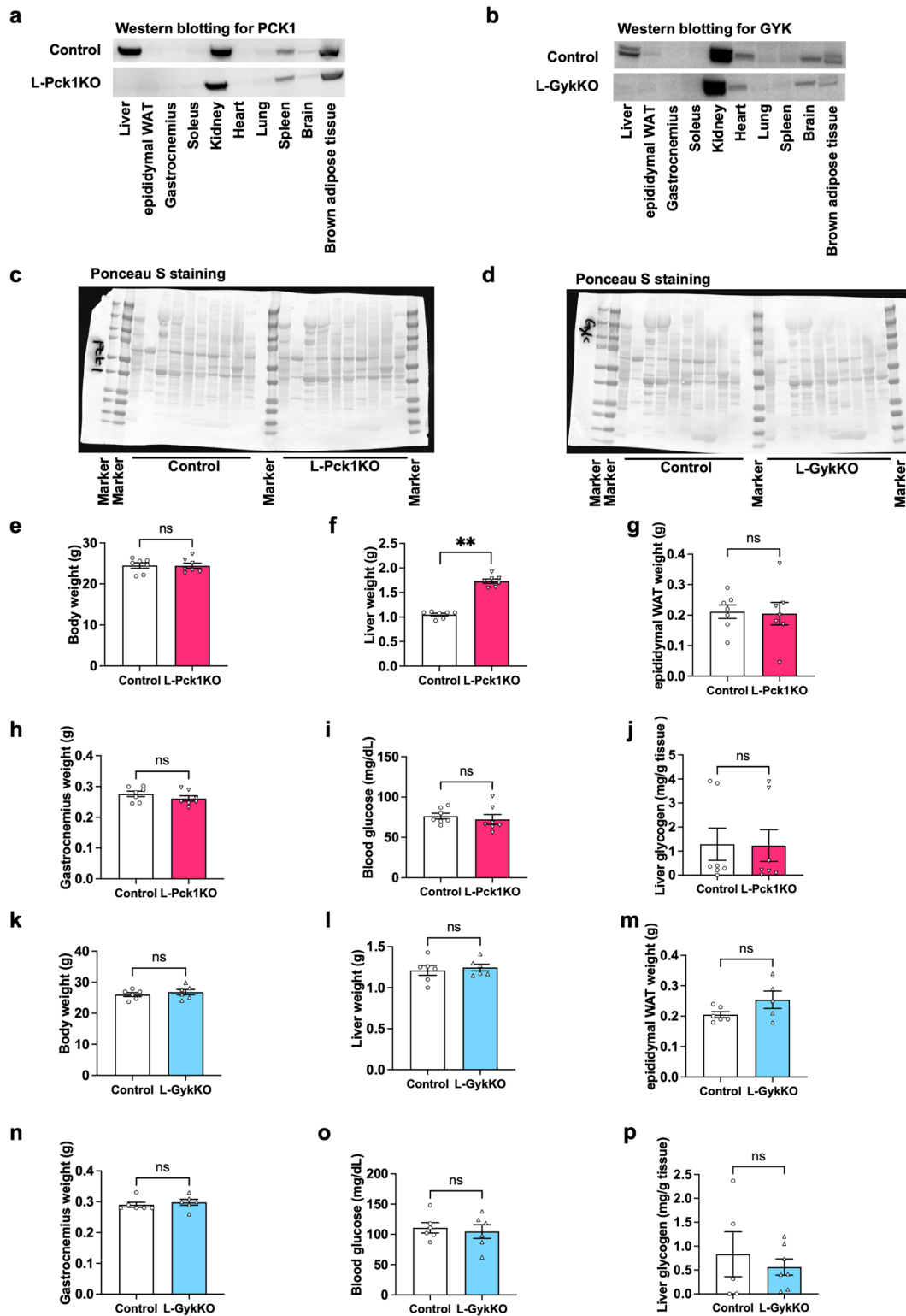
Low-intensity exercise for 60 minutes



Extended Data Fig. 1 | High-intensity exercise increases plasma lactate levels, while low-intensity exercise increases plasma glycerol levels.

(a–c) Concentrations of plasma lactate (a), plasma glycerol (b) and blood glucose (c) in male C57BL/6J wild-type mice before and after 20 min of high-intensity exercise. $n = 7$ per group; repeated measures two-way ANOVA followed by Holm–Šidák post hoc analysis (two-sided); (a) $**P = 0.0036$ vs Sedentary (Post), $^{##}P = 0.0031$ vs Pre (within Exercise). (d–f) Concentrations of plasma lactate

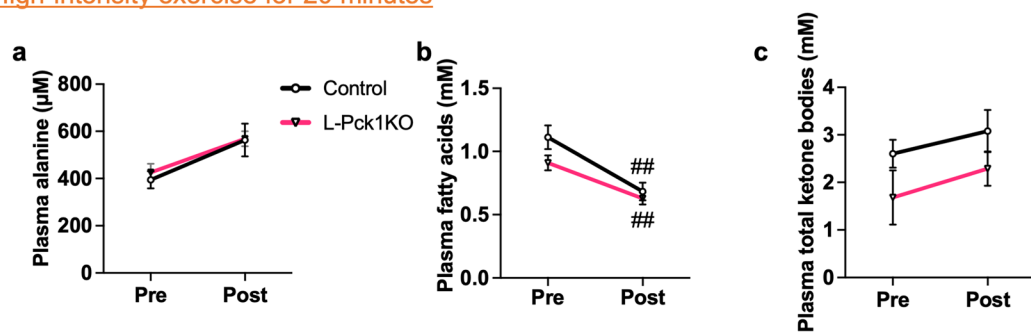
(d), plasma glycerol (e) and blood glucose (f) in male C57BL/6J wild-type mice before and after 60 min of low-intensity exercise. $n = 7$ per group; repeated measures two-way ANOVA followed by Holm–Šidák post hoc analysis (two-sided); (e) $*P = 0.0218$ vs Sedentary (Post), $^{##}P = 0.0069$ vs Pre (within Exercise). Experiments shown in (a–c) and (d–f) were conducted using distinct cohorts of biologically independent mice. All data are presented as means \pm s.e.m.



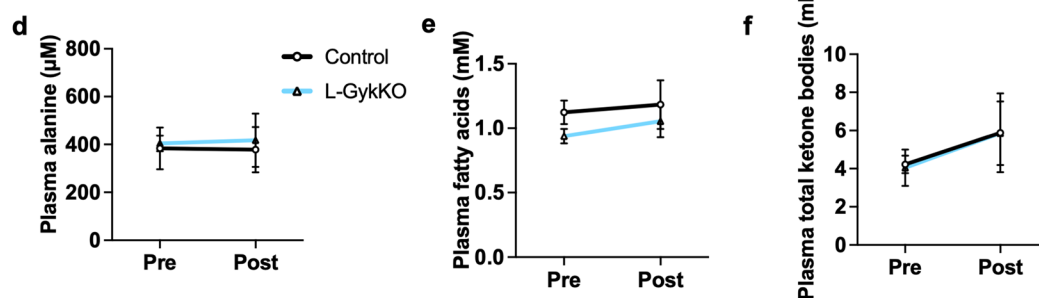
Extended Data Fig. 2 | Basic phenotypes of L-Pck1KO and L-GykKO mice under steady-state conditions. (a,b) Western blotting images for PCK1 (a) and GYK (b) in the indicated tissues after tamoxifen treatment are shown. The signals shown in (a) and (b) were each obtained from the same membrane within the respective panels. (c,d) The membranes used for western blotting were stained with Ponceau S to verify that the amounts of proteins loaded in the lane differed minimally between the same tissues from male mice with the indicated genotypes. (e–p) Weights of the whole body (e,k), liver (f,l), epididymal white

adipose tissue (WAT) (g,m) and gastrocnemius (h,n), as well as blood glucose levels (i,o) and liver glycogen contents (j,p) of male mice with the indicated genotypes under steady-state conditions. (e–j) $n = 7$ per group; (k–o) $n = 6$ per group (except for L-GykKO in (m), where $n = 5$ due to missing data); (p) $n = 5$ for Control, $n = 7$ for L-GykKO; two-tailed unpaired t -test; (f) $**P < 0.0001$. Experiments shown in (a,c), (b,d), (e–j), (k–o) and (p) were conducted using distinct cohorts of biologically independent mice. All data are presented as means \pm s.e.m. Each plot on the bar graph shows raw data.

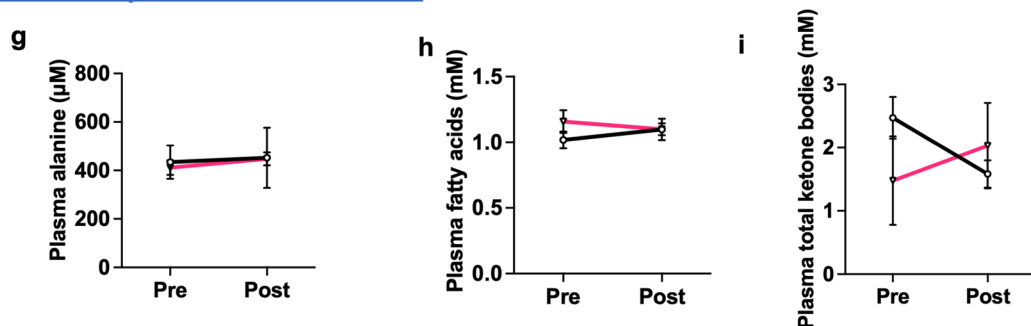
High-intensity exercise for 20 minutes



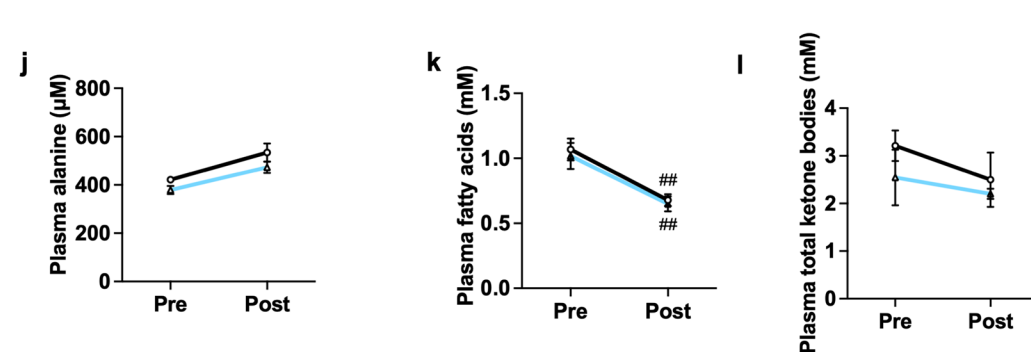
Low-intensity exercise for 60 minutes



Low-intensity exercise for 60 minutes

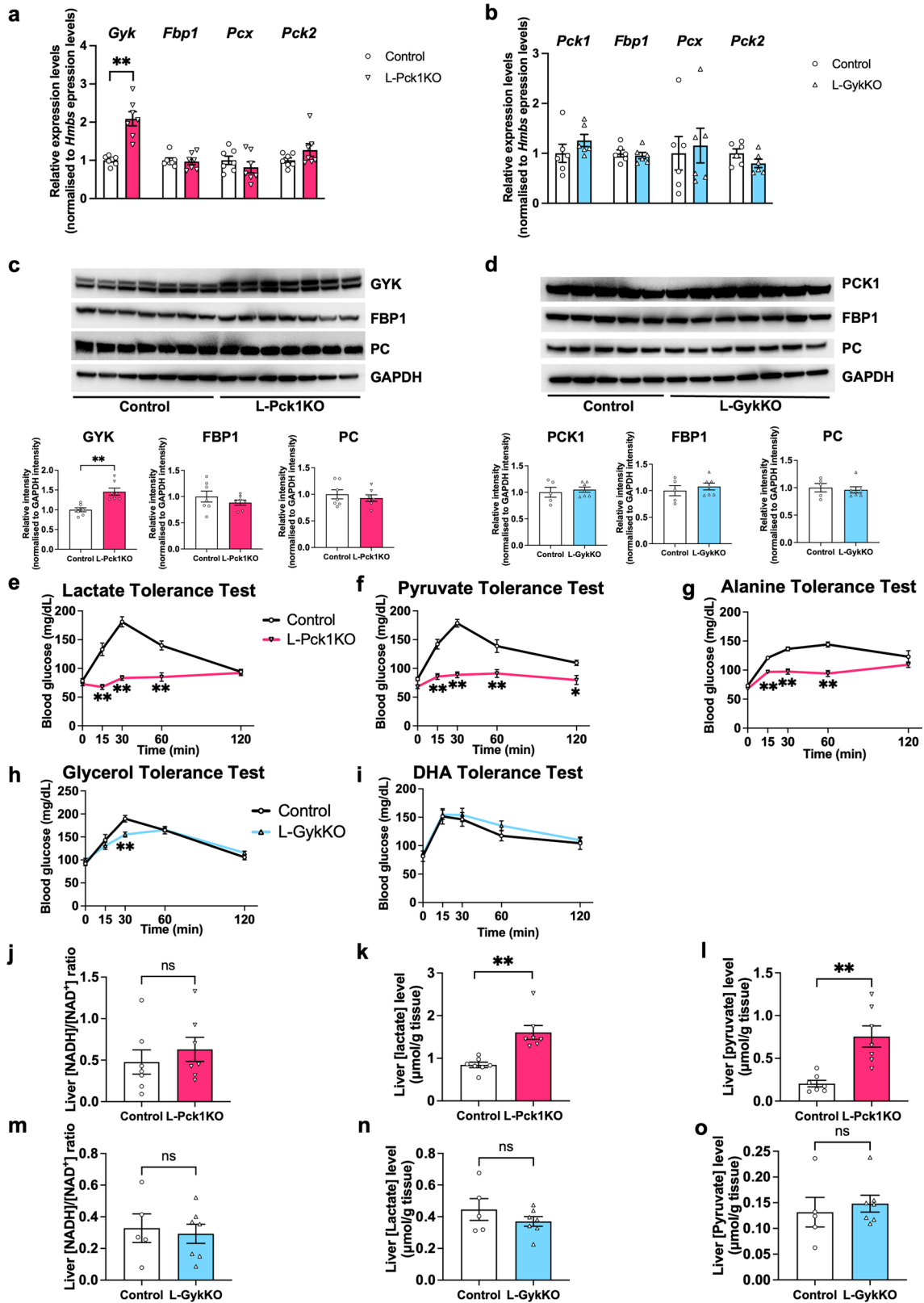


High-intensity exercise for 20 minutes



Extended Data Fig. 3 | L-Pck1KO and L-GykKO do not affect plasma concentrations of alanine, fatty acids, or ketone bodies during high-intensity and low-intensity exercise. (a–l) Plasma concentrations of alanine (a,d,g,j), fatty acids (b,e,h,k), and total ketone bodies (c,f,i,l) of male L-Pck1KO or L-GykKO mice in comparison with the corresponding controls were measured before and after the indicated type of exercise. (a,d,j) $n = 8$ per group; (b) $n = 9$ for Control, $n = 7$ for L-Pck1KO; (c) $n = 7$ for Control, $n = 5$ for L-Pck1KO; (e) $n = 9$ for Control, $n = 10$ for L-GykKO; (f) $n = 8$ for Control, $n = 7$ for L-GykKO; (g) $n = 7$ for Control, $n = 8$ for

L-Pck1KO; (h) $n = 12$ per group; (i) $n = 7$ for Control, $n = 5$ for L-Pck1KO; (k) $n = 6$ for Control, $n = 9$ for L-GykKO; (l) $n = 7$ for Control, $n = 5$ for L-GykKO; mixed-effects model (b,c,e–g,i,k,l) or repeated measures two-way ANOVA (a,d,j,h) followed by Holm–Šidák post hoc analysis (two-sided); (b) $^{##}P < 0.0001$ vs Pre (within Control), $^{##}P = 0.0002$ vs Pre (within L-Pck1KO); (k) $^{##}P < 0.0001$ vs Pre (within both Control and L-GykKO groups). All experiments shown in (a–l) were conducted using distinct cohorts of biologically independent mice. Data are presented as means \pm s.e.m.

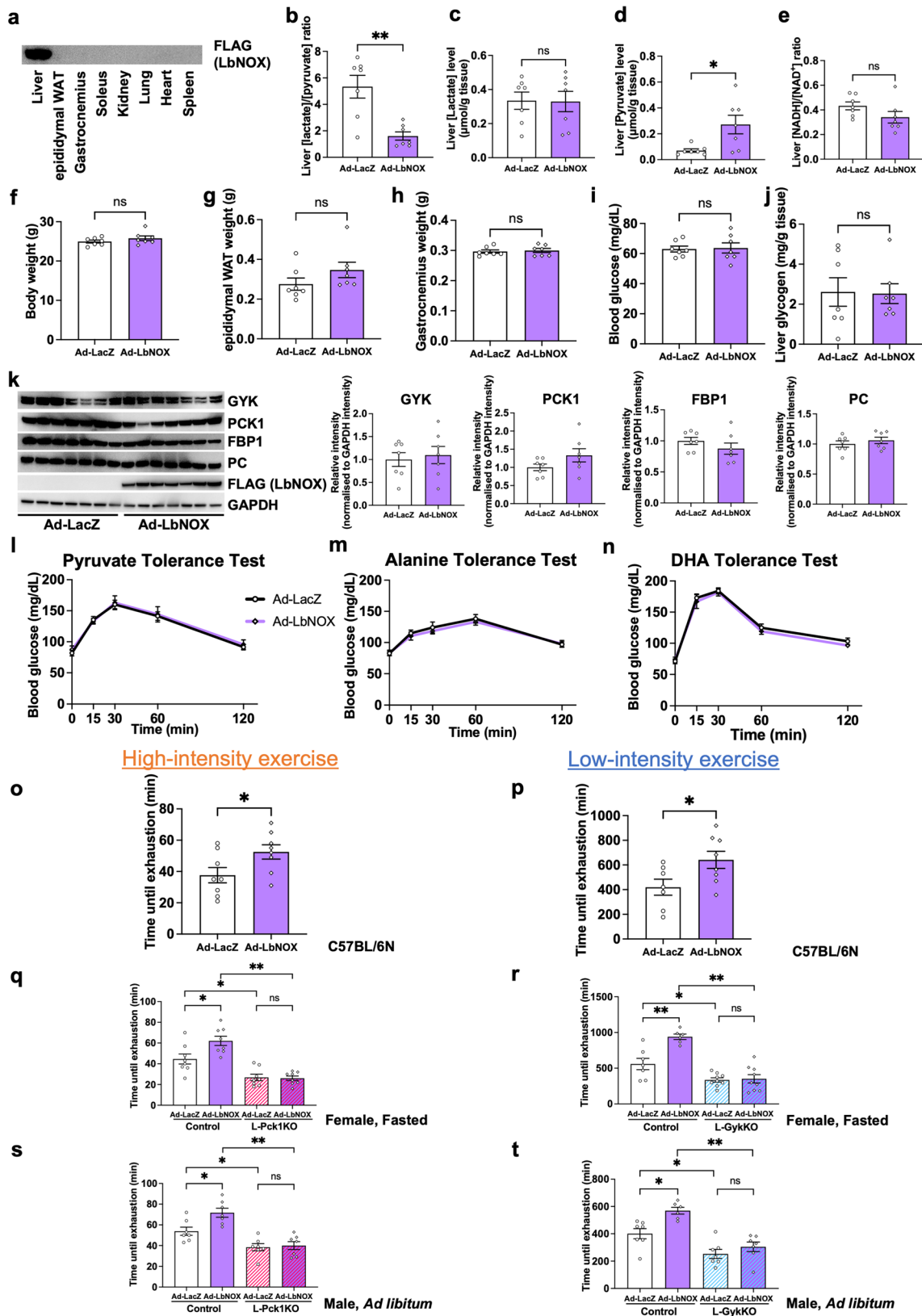


Extended Data Fig. 4 | See next page for caption.

Extended Data Fig. 4 | The alterations in gluconeogenic enzyme expressions and responses to gluconeogenic substrates in L-Pck1KO and L-GykKO mice.

(a,b) mRNA levels of the indicated gluconeogenic genes in the livers of male L-Pck1KO (a) and L-GykKO (b) in comparison with the corresponding controls. n = 7 (a) and 6 (b) per group; two-tailed unpaired *t*-test; (a) $^{**}P < 0.0001$ for Control vs L-Pck1KO (*Gyk* mRNA levels). (c,d) Western blots for liver gluconeogenic enzymes in male L-Pck1KO mice (c) and L-GykKO mice (d) in comparison to the corresponding controls. GAPDH was used as the loading control. Western blotting images for GAPDH in (c) and (d) correspond to those in Fig. 1c, e, respectively. Signals for each target protein in (c) and (d) were obtained from different membranes that were processed in parallel. Bar graphs represent the quantitative signal intensities of each band. (c) n = 7 per group; (d) n = 5 for Control, n = 7 for L-GykKO; two-tailed unpaired *t*-test; (c) $^{**}P < 0.0001$ for Control vs L-Pck1KO (GK protein levels). FBPI, fructose-1,6-bisphosphatase I; GAPDH, glyceraldehyde-3-phosphate dehydrogenase; GYK, glycerol kinase; PC, pyruvate carboxylase; PCK1, phosphoenolpyruvate carboxykinase-1. (e–i) Blood glucose levels of male L-Pck1KO and L-GykKO mice in comparison with the corresponding controls after administrations of the indicated gluconeogenic substrates.

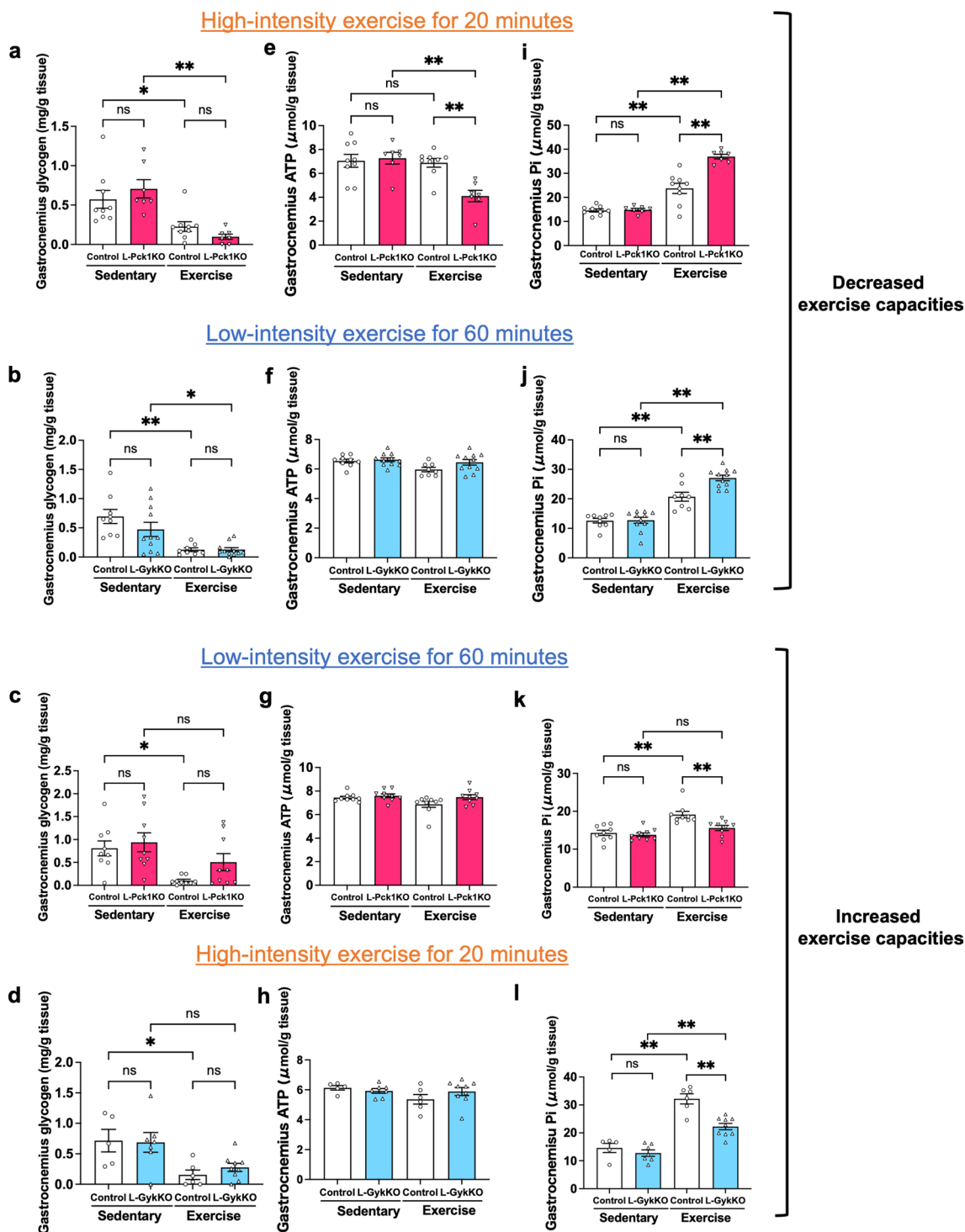
(e) n = 7 for Control, n = 6 for L-Pck1KO; (f) n = 5 for Control, n = 7 for L-Pck1KO; (g) n = 5 for Control, n = 7 for L-Pck1KO; (h) n = 8 per group; (i) n = 6 per group; mixed-effects model (e–g) or repeated measures two-way ANOVA (h,i) followed by Holm–Šidák post hoc analysis (two-sided); (e) $^{**}P < 0.0001$ vs Control (at 15, 30 and 60 min); (f) $^{**}P = 0.0002$, < 0.0001 and $= 0.0009$ vs Control (at 15, 30 and 60 min, respectively), $^{*}P = 0.0250$ vs Control (at 120 min); (g) $^{**}P = 0.0024$ vs Control (at 15 min), $^{**}P < 0.0001$ vs Control (at 30 and 60 min); (h) $^{**}P = 0.0005$ vs Control (at 30 min). All experiments shown in (e–i) were conducted using distinct cohorts of biologically independent mice. (j–o) The liver [NADH]/[NAD⁺] ratios (j,m) as well as the liver contents of lactate (k,n) and pyruvate (l,o) in male mice with the indicated genotypes are shown. The results of (k,l,n,o) were used for calculating the liver [lactate]/[pyruvate] ratios shown in Fig. 3g, h. (j–l) n = 7 per group; (m–o) n = 5 for Control, n = 7 for L-GykKO; two-tailed unpaired *t*-test; (k) $^{**}P = 0.0009$; (l) $^{**}P = 0.0011$. Experiments shown in (a,c), (b), (d), (e), (f), (g), (h), (i), (j–l) and (m–o) were conducted using distinct cohorts of biologically independent mice. All data are presented as means \pm s.e.m. Each plot on the bar graph shows raw data.



Extended Data Fig. 5 | See next page for caption.

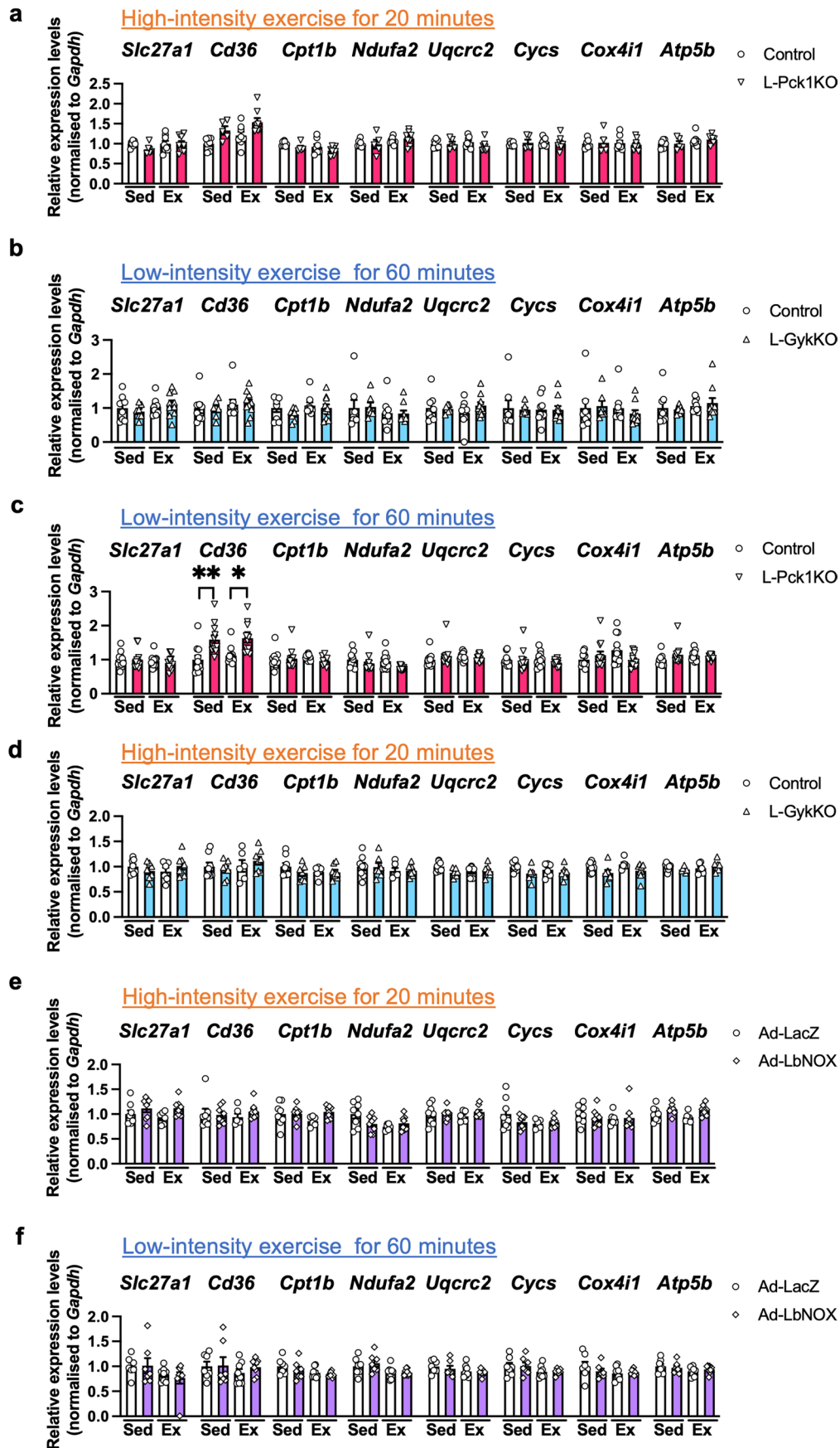
Extended Data Fig. 5 | Hepatic LbNOX expression enhances capacities for exercise of both intensities via enhanced redox-dependent gluconeogenesis, even in female mice or in the fed state. (a) Expressions of FLAG-tagged LbNOX in the indicated tissues from a male Ad-LbNOX mouse were examined by western blotting for FLAG. (b–e) The liver [lactate]/[pyruvate] ratios (b), lactate (c), pyruvate (d) and the [NADH]/[NAD⁺] ratios (e) in male Ad-LacZ and Ad-LbNOX mice under steady-state conditions are shown. n = 7 per group; two-tailed unpaired *t*-test; (b) ***P* = 0.0015; (d) **P* = 0.0178. (f–j) Weights of the whole body (f), epididymal white adipose tissue (WAT) (g) and gastrocnemius muscles (h), as well as blood glucose levels (i), and liver glycogen contents (j) were measured in male Ad-LacZ and Ad-LbNOX mice. n = 7 per group; two-tailed unpaired *t*-test. (k) Western blots for FLAG and the indicated gluconeogenic enzymes in the livers of male Ad-LacZ and Ad-LbNOX mice are shown. Signals for each target protein were obtained from different membranes that were processed in parallel. Bar graphs represent the quantitative signal intensities of each band. n = 7 per group; two-tailed unpaired *t*-test. FBPI, fructose-1,6-bisphosphatase 1; GAPDH, glyceraldehyde-3-phosphate dehydrogenase; GYK, glycerol kinase; PC, pyruvate carboxylase; PCK1, phosphoenolpyruvate carboxykinase-1. (l–n) Blood glucose levels of Ad-LacZ and Ad-LbNOX mice after intraperitoneal administration of pyruvate (l), alanine (m) and dihydroxyacetone (DHA) (n). (l) n = 7 for Ad-LacZ, n = 6 for Ad-LbNOX; (m,n) n = 7 per group. Mixed-effects model (l) or repeated measures two-way ANOVA (m,n) were performed (two-sided), without post hoc analysis due to the absence of significant interaction or group effects. (o,p) Times until exhaustion of C57BL/6 N mice administered with Ad-LacZ and Ad-

LbNOX were measured in high-intensity (o) and low-intensity (p) exercise. (o) n = 8 per group; (p) n = 7 for Ad-LacZ, n = 8 for Ad-LbNOX; two-tailed unpaired *t*-test; (o) **P* = 0.0441; (p) **P* = 0.0372. (q,r) Times until exhaustion of female mice with the indicated genotypes with the hepatic expression of LacZ or LbNOX were measured in high-intensity (q) and low-intensity (r) exercise under fasted conditions. (q) n = 8 per group; (r) n = 7 (Control + Ad-LacZ), n = 6 (Control + Ad-LbNOX), n = 9 each (L-GykKO + Ad-LacZ and Ad-LbNOX); one-way ANOVA followed by Tukey's post hoc analysis (two-sided); (q) **P* = 0.0145 for Ad-LacZ vs Ad-LbNOX (within Control), **P* = 0.0129 for Control vs L-Pck1KO (within Ad-LacZ), ***P* < 0.0001 for Control vs L-Pck1KO (within Ad-LbNOX); (r) ***P* = 0.0006 for Ad-LacZ vs Ad-LbNOX (within Control), **P* = 0.0326 for Control vs L-GykKO (within Ad-LacZ), **P* < 0.0001 for Control vs L-GykKO (within Ad-LbNOX). (s,t) Times until exhaustion of male mice with the indicated genotypes with the hepatic expression of LacZ or LbNOX were measured in high-intensity (s) and low-intensity (t) exercise under *ad libitum* conditions. n = 7 per group except for the Control + Ad-LbNOX group in (t), where n = 6; one-way ANOVA followed by Tukey's post hoc analysis (two-sided); (s) **P* = 0.0169 for Ad-LacZ vs Ad-LbNOX (within Control), **P* = 0.0453 for Control vs L-Pck1KO (within Ad-LacZ), ***P* < 0.0001 for Control vs L-Pck1KO (within Ad-LbNOX); (t) **P* = 0.0102 for Ad-LacZ vs Ad-LbNOX (within Control), **P* = 0.0202 for Control vs L-GykKO (within Ad-LacZ), ***P* < 0.0001 for Control vs L-GykKO (within Ad-LbNOX). Experiments shown in (a), (b–k), (l), (m), (n), (o), (p), (q), (r), (s) and (t) were conducted using distinct cohorts of biologically independent mice. All data are presented as means ± s.e.m. Each plot on the bar graph shows raw data.



Extended Data Fig. 6 | Muscle metabolite alterations during high-intensity and low-intensity exercise. (a–i) Contents of glycogen (a–d), ATP (e–h) and Pi (i–l) in the gastrocnemius were measured in male L-Pck1KO and L-GykKO mice in comparison with those of the corresponding controls under sedentary conditions and with the indicated intensity of exercise. (a, e, i) $n = 9$ for Control in both Sedentary and Exercise groups, $n = 7$ for L-Pck1KO in both Sedentary and Exercise groups; (b, f, j) $n = 9$ for Sedentary-Control, $n = 8$ for Exercise-Control, $n = 11$ for L-GykKO in both Sedentary and Exercise groups; (c, g, k) $n = 9$ per group; (d, h, l) $n = 5$ for Sedentary-Control, $n = 7$ for Sedentary-L-GykKO, $n = 6$ for Exercise-Control, $n = 9$ for Exercise-L-GykKO; one-way ANOVA followed by Tukey's post hoc analysis (two-sided); (a) $*P = 0.0350$ for Sedentary vs Exercise (within Control), $**P = 0.0006$ for Sedentary vs Exercise (within L-Pck1KO);

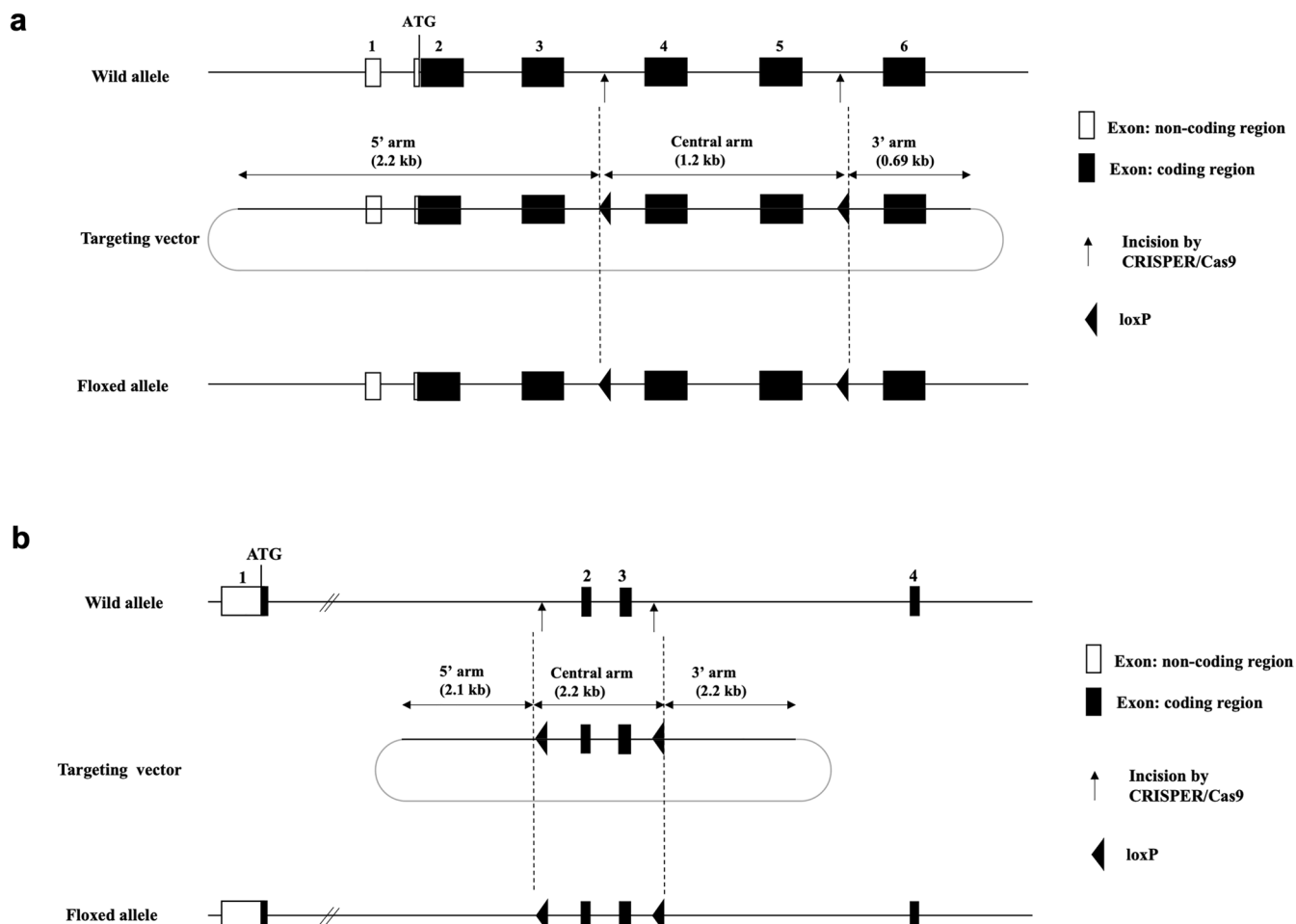
(b) $**P = 0.0012$ for Sedentary vs Exercise (within Control), $*P = 0.0351$ for Sedentary vs Exercise (within L-GykKO); (c) $*P = 0.0210$ for Sedentary vs Exercise (within Control); (d) $*P = 0.0349$ for Sedentary vs Exercise (within Control); (e) $**P = 0.0007$ for Sedentary vs Exercise (within L-Pck1KO), $**P = 0.0015$ for Control vs L-Pck1KO (within Exercise); (i) $**P = 0.0001$ for Sedentary vs Exercise (within Control), $**P < 0.0001$ for Sedentary vs Exercise (within L-Pck1KO) and for Control vs L-Pck1KO (within Exercise); (j) $**P < 0.0001$ for all indicated comparisons; (l) $**P < 0.0001$ for Sedentary vs Exercise (within Control), $**P = 0.0002$ for Sedentary vs Exercise (within L-GykKO) and for Control vs L-GykKO (within Exercise). Experiments shown in (a, e, i), (b, f, j), (c, g, k) and (d, h, l) were conducted using distinct cohorts of biologically independent mice. Data are presented as means \pm s.e.m. Each plot on the bar graph shows raw data.



Extended Data Fig. 7 | See next page for caption.

Extended Data Fig. 7 | Liver-specific modulations of gluconeogenesis have minimal effects on the muscular expressions of genes related to fatty acid oxidation and the mitochondrial electron transport chain. (a–f) Expression levels of mRNA related to fatty acid oxidation and the mitochondrial electron transport chain (ETC) of male L-Pck1KO, L-GyckKO and Ad-LbNOX mouse gastrocnemius, for comparison with the corresponding controls, were measured under sedentary conditions and the indicated intensity of exercise. Expression levels of mRNA were normalised to *glyceraldehyde-3-phosphate dehydrogenase* (*Gapdh*) expression levels. Sed, sedentary; Ex, exercised. (a) n = 7 for Sed-Control, n = 5 for Sed-L-Pck1KO, n = 8 for both Ex-Control and Ex-L-Pck1KO; (b) n = 8 for

Sed-Control, n = 7 for Sed-L-GyckKO, n = 9 for Ex-Control, n = 10 for Ex-L-GyckKO; (c) n = 12 per group, except for Sed-Control (n = 11); (d) n = 8 for Sed-Control and Ex-L-GyckKO, n = 7 for Sed-L-GyckKO, n = 6 for Ex-Control; (e) n = 8 per group, except for Ex-Ad-LacZ (n = 6); (f) n = 7 for Sed-Ad-LacZ and Sed-Ad-LbNOX, n = 8 for Ex-Ad-LacZ and Ex-Ad-LbNOX; one-way ANOVA followed by Tukey's post hoc analysis (two-sided); (c) ** $P = 0.0039$ for Control vs L-Pck1KO (within Sed), * $P = 0.0116$ for Control vs L-Pck1KO (within Ex). All experiments shown in (a–f) were conducted using distinct cohorts of biologically independent mice. Data are presented as means \pm s. e. m. Each plot on the bar graph shows raw data.



Extended Data Fig. 8 | Schematic representations of the vectors used for the generation of *Pck1*- and *Gyk*-floxed mice. (a) Schematic representation of the CRISPR/Cas9-mediated gene deletion used for the generation of *Pck1*-floxed mice. Each box represents one exon (numbered). The black boxes represent the *Pck1* coding exons, and the open boxes the non-coding regions. Two mouse genomic sequences (5'-TAG CTG TAG CTA TGG TTC CG-3' and 5'-AAG GTC TGG GAA AGC GCG TA-3') in introns 3 and 5, respectively, of *Pck1* were selected as guide RNA targets (Arrows). The targeting vector contains six exons of the *Pck1* gene, the fourth and fifth of which are flanked by loxP sites. Homologous recombination between the targeting vector and the *Pck1* locus was confirmed

by polymerase chain reaction (PCR). **(b)** Schematic representation of the CRISPR/Cas9-mediated gene deletion used for the generation of *Gyk*-floxed mice. Each box represents one exon (numbered). The black boxes represent the *Gyk* coding exons and the open boxes indicate the non-coding regions. Two mouse genomic sequences (5'-AGC GTA TCG TTC CCA GAC AT-3') and (5'-TCA ACC AAC CAT GGC AGC AT-3') in introns 1 and 3, respectively, of *Gyk* were selected as guide RNA targets (Arrows). The targeting vector contains the second and third exons of the *Gyk* gene, flanked by loxP sites. Homologous recombination between the targeting vector and the *Gyk* locus was confirmed by PCR. The details of the methods employed are described in the Materials & Methods section.

Reporting Summary

Nature Portfolio wishes to improve the reproducibility of the work that we publish. This form provides structure for consistency and transparency in reporting. For further information on Nature Portfolio policies, see our [Editorial Policies](#) and the [Editorial Policy Checklist](#).

Statistics

For all statistical analyses, confirm that the following items are present in the figure legend, table legend, main text, or Methods section.

n/a Confirmed

- | | | |
|-------------------------------------|-------------------------------------|--|
| <input type="checkbox"/> | <input checked="" type="checkbox"/> | The exact sample size (n) for each experimental group/condition, given as a discrete number and unit of measurement |
| <input type="checkbox"/> | <input checked="" type="checkbox"/> | A statement on whether measurements were taken from distinct samples or whether the same sample was measured repeatedly |
| <input type="checkbox"/> | <input checked="" type="checkbox"/> | The statistical test(s) used AND whether they are one- or two-sided
<i>Only common tests should be described solely by name; describe more complex techniques in the Methods section.</i> |
| <input checked="" type="checkbox"/> | <input type="checkbox"/> | A description of all covariates tested |
| <input type="checkbox"/> | <input checked="" type="checkbox"/> | A description of any assumptions or corrections, such as tests of normality and adjustment for multiple comparisons |
| <input type="checkbox"/> | <input checked="" type="checkbox"/> | A full description of the statistical parameters including central tendency (e.g. means) or other basic estimates (e.g. regression coefficient) AND variation (e.g. standard deviation) or associated estimates of uncertainty (e.g. confidence intervals) |
| <input type="checkbox"/> | <input checked="" type="checkbox"/> | For null hypothesis testing, the test statistic (e.g. F , t , r) with confidence intervals, effect sizes, degrees of freedom and P value noted
<i>Give P values as exact values whenever suitable.</i> |
| <input checked="" type="checkbox"/> | <input type="checkbox"/> | For Bayesian analysis, information on the choice of priors and Markov chain Monte Carlo settings |
| <input checked="" type="checkbox"/> | <input type="checkbox"/> | For hierarchical and complex designs, identification of the appropriate level for tests and full reporting of outcomes |
| <input checked="" type="checkbox"/> | <input type="checkbox"/> | Estimates of effect sizes (e.g. Cohen's d , Pearson's r), indicating how they were calculated |

Our web collection on [statistics for biologists](#) contains articles on many of the points above.

Software and code

Policy information about [availability of computer code](#)

Data collection

Data analysis

For manuscripts utilizing custom algorithms or software that are central to the research but not yet described in published literature, software must be made available to editors and reviewers. We strongly encourage code deposition in a community repository (e.g. GitHub). See the Nature Portfolio [guidelines for submitting code & software](#) for further information.

Data

Policy information about [availability of data](#)

All manuscripts must include a [data availability statement](#). This statement should provide the following information, where applicable:

- Accession codes, unique identifiers, or web links for publicly available datasets
- A description of any restrictions on data availability
- For clinical datasets or third party data, please ensure that the statement adheres to our [policy](#)

All data supporting the findings of this study are available within the manuscript. Raw data are presented in bar graphs, and source data are provided with this paper. No external datasets were generated or analyzed during the current study.

Research involving human participants, their data, or biological material

Policy information about studies with [human participants or human data](#). See also policy information about [sex, gender \(identity/presentation\), and sexual orientation](#) and [race, ethnicity and racism](#).

Reporting on sex and gender	<input type="text" value="not applicable"/>
Reporting on race, ethnicity, or other socially relevant groupings	<input type="text" value="not applicable"/>
Population characteristics	<input type="text" value="not applicable"/>
Recruitment	<input type="text" value="not applicable"/>
Ethics oversight	<input type="text" value="not applicable"/>

Note that full information on the approval of the study protocol must also be provided in the manuscript.

Field-specific reporting

Please select the one below that is the best fit for your research. If you are not sure, read the appropriate sections before making your selection.

Life sciences Behavioural & social sciences Ecological, evolutionary & environmental sciences

For a reference copy of the document with all sections, see [nature.com/documents/nr-reporting-summary-flat.pdf](https://www.nature.com/documents/nr-reporting-summary-flat.pdf)

Life sciences study design

All studies must disclose on these points even when the disclosure is negative.

Sample size	No statistical method was used to predetermine sample size. Sample sizes were based on our prior experience with similar experiments and are consistent with those reported in previous publications.
Data exclusions	Mice with abnormal body weights were excluded prior to the experiments. In the isotopic flux analysis (Figures 2i–m), mice with >10% weight loss compared to pre-surgery or with technical failures (e.g., catheter withdrawal) were excluded. In Extended Data Figure 2m, one epididymal WAT weight value was missing (not recorded) in the L-GykKO group and was excluded. No other data were excluded.
Replication	Key experiments with exercise capacities and changes of plasma metabolite concentrations (Figures 1f–m, 2a–h, 4c–l), and experiments related to gluconeogenic responses (Figures 3a–j, 4a,b) were replicated in independent experiments. In main figures, experiments with isotopic flux (Figures 2i–m) were not replicated at this stage, due to its extended duration of the experiments.
Randomization	Mice of the same sex and age were used in each experiment. Animals were randomly assigned to experimental groups after matching for body weight.
Blinding	Formal blinding was not performed due to technical constraints requiring knowledge of group allocation. For example, treadmill running involved simultaneous exercise of multiple mice, making it necessary to identify individual animals during the experiment.

Reporting for specific materials, systems and methods

We require information from authors about some types of materials, experimental systems and methods used in many studies. Here, indicate whether each material, system or method listed is relevant to your study. If you are not sure if a list item applies to your research, read the appropriate section before selecting a response.

Materials & experimental systems

- | | |
|-------------------------------------|---|
| n/a | Included in the study |
| <input type="checkbox"/> | <input checked="" type="checkbox"/> Antibodies |
| <input checked="" type="checkbox"/> | <input type="checkbox"/> Eukaryotic cell lines |
| <input checked="" type="checkbox"/> | <input type="checkbox"/> Palaeontology and archaeology |
| <input type="checkbox"/> | <input checked="" type="checkbox"/> Animals and other organisms |
| <input checked="" type="checkbox"/> | <input type="checkbox"/> Clinical data |
| <input checked="" type="checkbox"/> | <input type="checkbox"/> Dual use research of concern |
| <input checked="" type="checkbox"/> | <input type="checkbox"/> Plants |

Methods

- | | |
|-------------------------------------|---|
| n/a | Included in the study |
| <input checked="" type="checkbox"/> | <input type="checkbox"/> ChIP-seq |
| <input checked="" type="checkbox"/> | <input type="checkbox"/> Flow cytometry |
| <input checked="" type="checkbox"/> | <input type="checkbox"/> MRI-based neuroimaging |

Antibodies

Antibodies used	<p>All antibodies were used for western blotting.</p> <p>Primary antibodies: GAPDH (#5174S, Cell Signaling Technology; 1:2,000) GYK (ab126599, Abcam; 1:2,000) PCK1 (16754-1-AP, Proteintech; 1:2,000) PC (16588-1-AP, Proteintech; 1:2,000) FBP1 (ab109732, Abcam; 1:2,000) FLAG (#2368, Cell Signaling Technology; 1:2,000)</p> <p>Secondary antibody: anti-rabbit horseradish peroxidase-linked IgG secondary antibody (NA9340V, GE Health Care Japan; 1:10,000)</p>
Validation	<p>All antibodies were commercially obtained. See following links for validation.</p> <p>Primary antibodies: GAPDH (#5174S, Cell Signaling Technology) https://www.cellsignal.com/products/primary-antibodies/gapdh-d16h11-xp-rabbit-mab/5174?site-search-type=Products&N=4294956287&Ntt=5174s&fromPage=plp&_requestid=688970 GYK (ab126599, Abcam) https://www.abcam.com/products/primary-antibodies/glycerol-kinase-antibody-epr6567-ab126599.html PCK1 (16754-1-AP, Proteintech) https://www.ptglab.com/products/PCK1-Antibody-16754-1-AP.htm PC (16588-1-AP, Proteintech) https://www.ptglab.com/products/PC-Antibody-16588-1-AP.htm FBP1 (ab109732, Abcam) https://www.abcam.co.jp/products/primary-antibodies/fbp1-antibody-epr4620-ab109732.html FLAG (#2368, Cell Signaling Technology) https://www.cellsignal.com/products/primary-antibodies/dykdddk-tag-antibody-binds-to-same-epitope-as-sigma-aldrich-anti-flag-m2-antibody/2368?srsltid=AfmBOopjH36gUUscbxwxE_2fdHnPxsObGVFfesD7qc2m3VBM6rLQa5I</p> <p>Secondary antibody: anti-rabbit horseradish peroxidase-linked IgG secondary antibody (NA9340V, GE Health Care Japan) https://gels.yilimart.com/Assets/Images/doc/file/NA934-1ML_INSTRUCTION_09.PDF</p>

Animals and other research organisms

Policy information about [studies involving animals](#); [ARRIVE guidelines](#) recommended for reporting animal research, and [Sex and Gender in Research](#)

Laboratory animals	<p>Mice were housed in groups of 2-5 animals per cage under a 12-hour light/dark cycle at an ambient temperature of 23-27°C and 40-60% humidity. All experiments were conducted at 16-18 weeks of age. Male C57BL/6J and C57BL/6N mice at 8-12 weeks of age were purchased from CLEA Japan. L-GykKO and L-Pck1KO mice were obtained by crossing SA-CreERT2 mice with Gyk- and Pck1-floxed mice, respectively. All mice were of C57BL/6 background. The detailed methods for generating Gyk- and Pck1-floxed mice are within the manuscript.</p>
Wild animals	<p>No wild animals were used in this study.</p>
Reporting on sex	<p>Male and female mice were used in this study as indicated.</p>
Field-collected samples	<p>No field-collected samples were used in this study.</p>
Ethics oversight	<p>All animal experiments were conducted in accordance with the Tohoku University institutional guidelines. Ethics approval was obtained from the Institutional Animal Care and Use Committee of the Tohoku University Environmental & Safety Committee. Generation of Gyk-floxed mice was performed at Trans Genic Inc. (Fukuoka, Japan) with institutional Animal Research Committee approval. Generation of Pck1-floxed mice was performed at the University of Tsukuba (Ibaraki, Japan) with the approval by the University of Tsukuba Animal Experiment Committee.</p>

Note that full information on the approval of the study protocol must also be provided in the manuscript.